Effects of composite rheology on plate-like behavior in global-scale mantle convection

Maelis Arnould[1], Tobias Rolf[2], and Antonio Manjón-Cabeza Córdoba[3]

[1]Université Claude Bernard Lyon 1
[2]University of Oslo
[3]University College London

May 4, 2023

Abstract

Earthâ\euros upper mantle rheology controls lithosphere-asthenosphere coupling and thus surface tectonics. Rock deformation experiments and seismic anisotropy measurements indicate that composite rheology (co-existing diffusion and dislocation creep) occurs in the Earth's uppermost mantle, potentially affecting convection and surface tectonics. Here, we investigate how the spatio-temporal distribution of dislocation creep in an otherwise diffusion-creep-controlled mantle impacts the planform of convection and the planetary tectonic regime as a function of the lithospheric yield strength in numerical models of mantle convection self-generating plate-like tectonics. The low upper-mantle viscosities caused by zones of substantial dislocation creep produce contrasting effects on surface dynamics. For strong lithosphere (yield strength $>$35 MPa), the large lithosphere-asthenosphere viscosity contrasts promote stagnant-lid convection. In contrast, the increase of upper mantle convective vigor enhances plate mobility for lithospheric strength $<$35 MPa. For the here-used model assumptions, composite rheology does not facilitate the onset of plate-like behavior at large lithospheric strength.

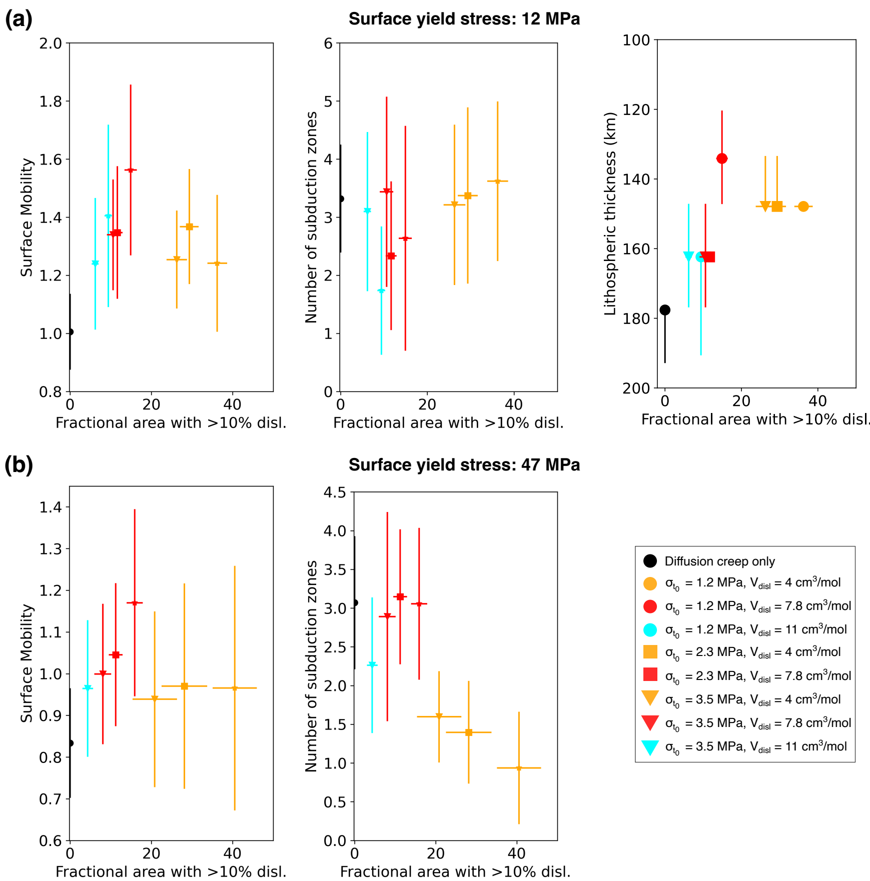

(a)
Surface yield stress: 12 MPa
Surface Mobility
Number of subduction zones
Lithospheric thickness (km)
Fractional area with >10% disl.
(b)
Surface yield stress: 47 MPa
Surface Mobility
Number of subduction zones
Fractional area with >10% disl.
Diffusion creep only
σ_{t_0} = 1.2 MPa, V_{disl} = 4 cm^3/mol
σ_{t_0} = 1.2 MPa, V_{disl} = 7.8 cm^3/mol
σ_{t_0} = 1.2 MPa, V_{disl} = 11 cm^3/mol
σ_{t_0} = 2.3 MPa, V_{disl} = 4 cm^3/mol
σ_{t_0} = 2.3 MPa, V_{disl} = 7.8 cm^3/mol
σ_{t_0} = 3.5 MPa, V_{disl} = 4 cm^3/mol
σ_{t_0} = 3.5 MPa, V_{disl} = 7.8 cm^3/mol
σ_{t_0} = 3.5 MPa, V_{disl} = 11 cm^3/mol

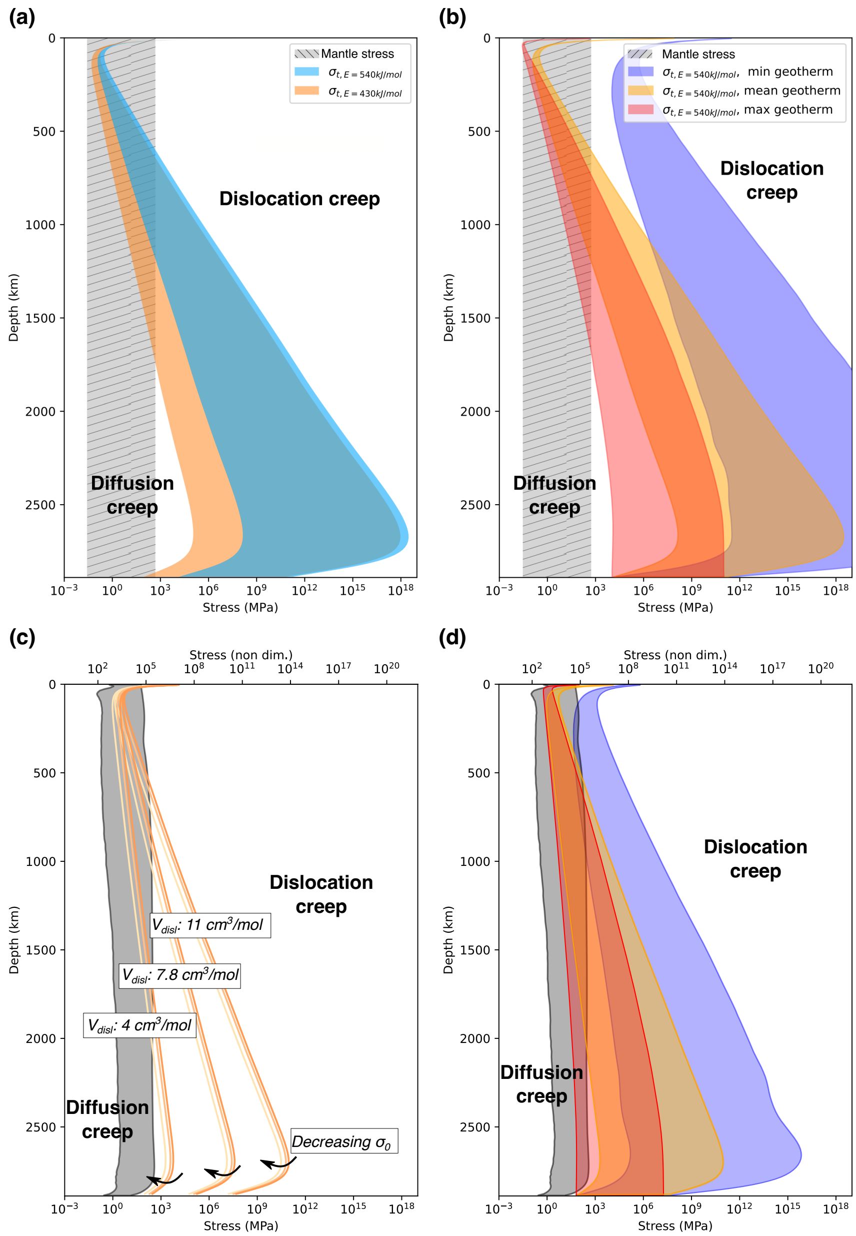

(a)
Mantle stress
$\sigma_{t,E=540kJ/mol}$
$\sigma_{t,E=430kJ/mol}$
Dislocation creep
Diffusion creep
Depth (km)
Stress (MPa)
(b)
Mantle stress
$\sigma_{t,E=540kJ/mol}$, min geotherm
$\sigma_{t,E=540kJ/mol}$, mean geotherm
$\sigma_{t,E=540kJ/mol}$, max geotherm
Dislocation creep
Diffusion creep
Depth (km)
Stress (MPa)
(c)
Stress (non dim.)
V_{disl}: 11 cm^3/mol
V_{disl}: 7.8 cm^3/mol
V_{disl}: 4 cm^3/mol
Decreasing σ_0
Dislocation creep
Diffusion creep
Depth (km)
Stress (MPa)
(d)
Stress (non dim.)
Dislocation creep
Diffusion creep
Depth (km)
Stress (MPa)

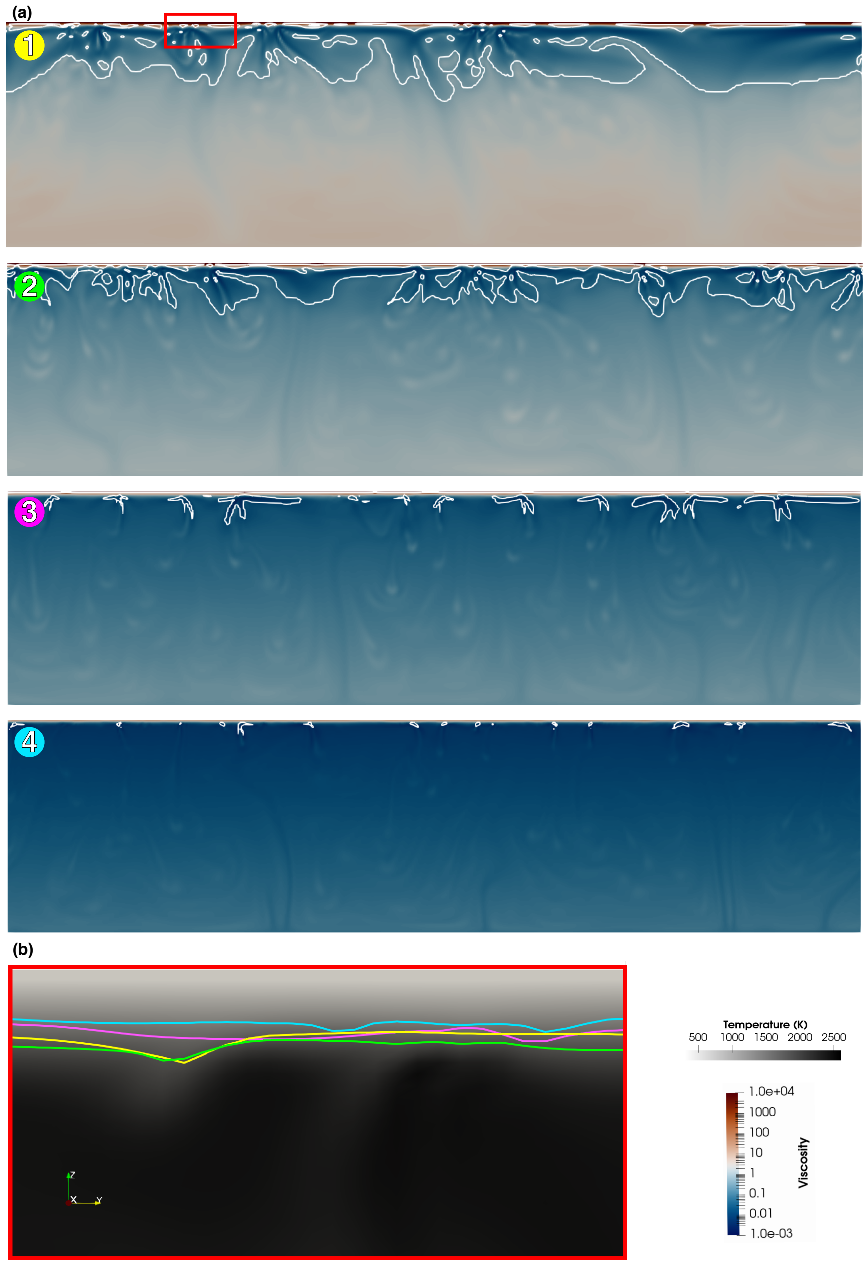

(a)
1
2
3
4
(b)
Temperature (K)
500 1000 1500 2000 2500
1.0e+04
1000
100
10
1
0.1
0.01
1.0e-03
Viscosity

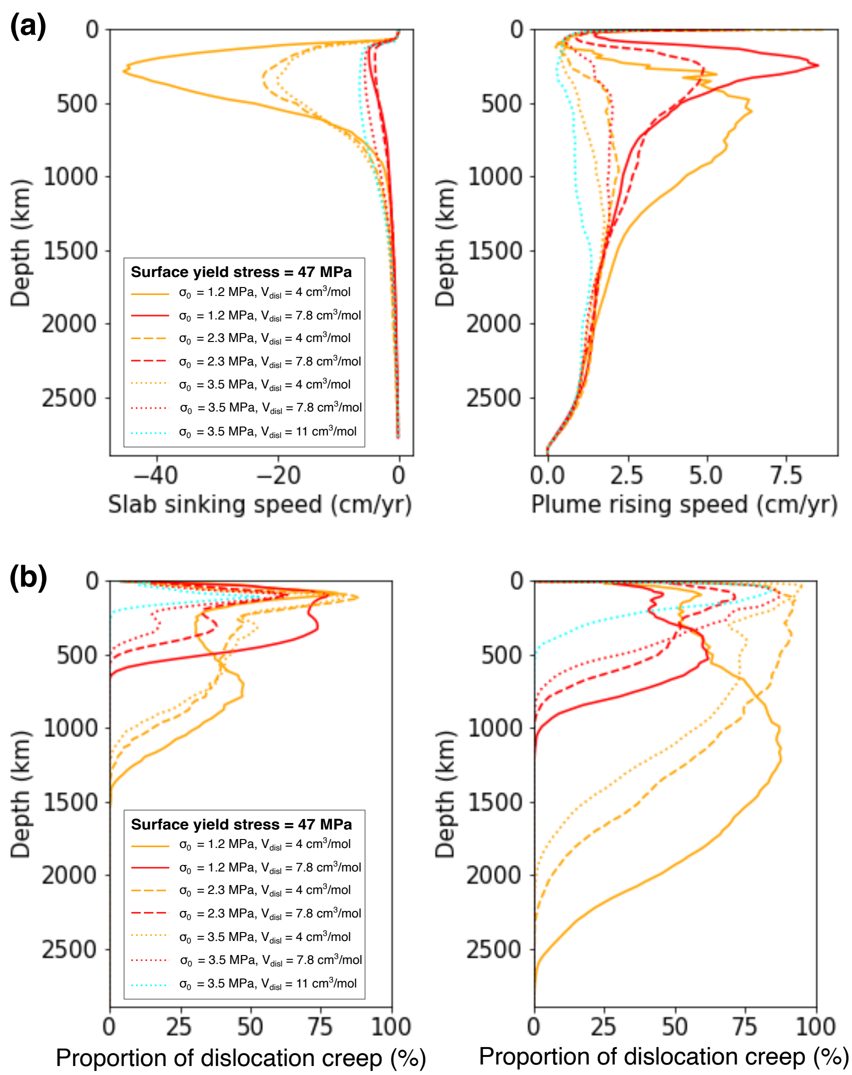

(a)
Depth (km)
Slab sinking speed (cm/yr)
Plume rising speed (cm/yr)
(b)
Proportion of dislocation creep (%)
Surface yield stress = 47 MPa
σ_0 = 1.2 MPa, V_{disl} = 4 cm^3/mol
σ_0 = 1.2 MPa, V_{disl} = 7.8 cm^3/mol
σ_0 = 2.3 MPa, V_{disl} = 4 cm^3/mol
σ_0 = 2.3 MPa, V_{disl} = 7.8 cm^3/mol
σ_0 = 3.5 MPa, V_{disl} = 4 cm^3/mol
σ_0 = 3.5 MPa, V_{disl} = 7.8 cm^3/mol
σ_0 = 3.5 MPa, V_{disl} = 11 cm^3/mol

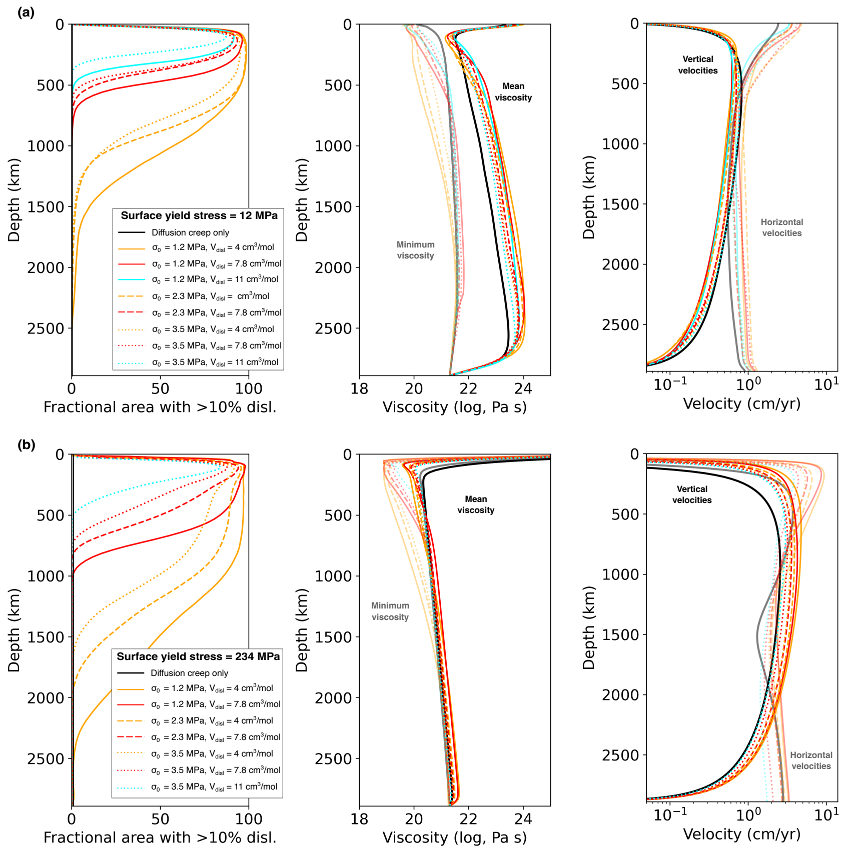

(a)
Surface yield stress = 12 MPa
Diffusion creep only
σ_0 = 1.2 MPa, V_{disl} = 4 cm^3/mol
σ_0 = 1.2 MPa, V_{disl} = 7.8 cm^3/mol
σ_0 = 1.2 MPa, V_{disl} = 11 cm^3/mol
σ_0 = 2.3 MPa, V_{disl} = cm^3/mol
σ_0 = 2.3 MPa, V_{disl} = 7.8 cm^3/mol
σ_0 = 3.5 MPa, V_{disl} = 4 cm^3/mol
σ_0 = 3.5 MPa, V_{disl} = 7.8 cm^3/mol
σ_0 = 3.5 MPa, V_{disl} = 11 cm^3/mol
Depth (km)
Fractional area with >10% disl.
Mean viscosity
Minimum viscosity
Viscosity (log, Pa s)
Vertical velocities
Horizontal velocities
Velocity (cm/yr)
(b)
Surface yield stress = 234 MPa
Diffusion creep only
σ_0 = 1.2 MPa, V_{disl} = 4 cm^3/mol
σ_0 = 1.2 MPa, V_{disl} = 7.8 cm^3/mol
σ_0 = 2.3 MPa, V_{disl} = 4 cm^3/mol
σ_0 = 2.3 MPa, V_{disl} = 7.8 cm^3/mol
σ_0 = 3.5 MPa, V_{disl} = 4 cm^3/mol
σ_0 = 3.5 MPa, V_{disl} = 7.8 cm^3/mol
σ_0 = 3.5 MPa, V_{disl} = 11 cm^3/mol
Depth (km)
Fractional area with >10% disl.
Mean viscosity
Minimum viscosity
Viscosity (log, Pa s)
Vertical velocities
Horizontal velocities
Velocity (cm/yr)

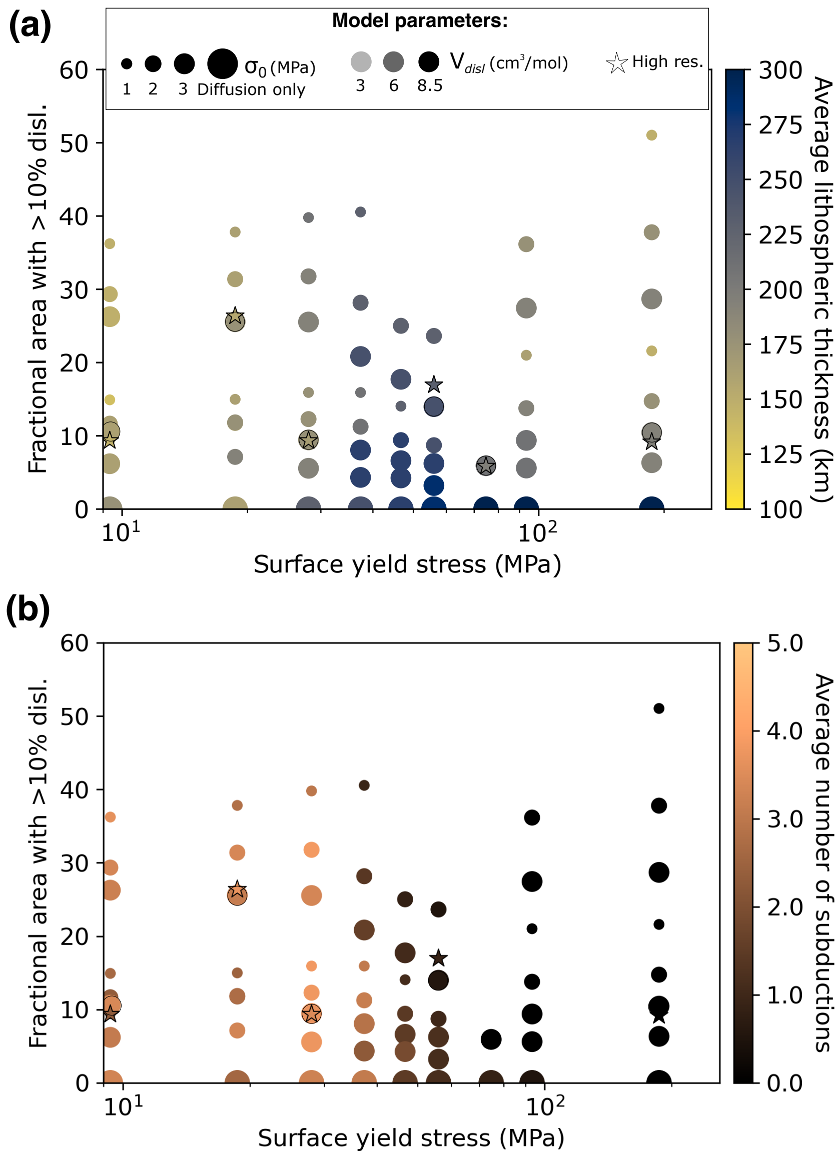

(a)
Model parameters:
σ0 (MPa)
1 2 3 Diffusion only
Vdisl (cm³/mol)
3 6 8.5
High res.
Fractional area with >10% disl.
Surface yield stress (MPa)
Average lithospheric thickness (km)
(b)
Fractional area with >10% disl.
Surface yield stress (MPa)
Average number of subductions

Effects of composite rheology on plate-like behavior in global-scale mantle convection

Maëlis Arnould [1,2], Tobias Rolf [2,3] and Antonio Manjón-Cabeza Córdoba [2,4,5]

[1]University of Lyon, UCBL, ENSL, UJM, CNRS 5276, Laboratoire de Géologie de Lyon - Terre, Planètes, Environnement, Lyon, France

[2]Centre for Earth Evolution and Dynamics, Department of Geosciences, University of Oslo, Blindern, Oslo, Norway

[3]Institute of Geophysics, University of Münster, Germany

[4]Andalusian Earth Sciences Institute, University of Grenada, Spain

[5]Department of Earth Sciences, University College London, UK

Key Points:

- Uppermost mantle viscosity variations induced by composite rheology control surface tectonics
- Composite rheology can impede or enhance plate mobility depending on lithospheric strength
- Composite rheology does not facilitate the onset of subduction for large yield stress

Corresponding author: Maelis Arnould, `maelis.arnould@univ-lyon1.fr`

Abstract

Earth's upper mantle rheology controls lithosphere-asthenosphere coupling and thus surface tectonics. Rock deformation experiments and seismic anisotropy measurements indicate that composite rheology (co-existing diffusion and dislocation creep) occurs in the Earth's uppermost mantle, potentially affecting convection and surface tectonics. Here, we investigate how the spatio-temporal distribution of dislocation creep in an otherwise diffusion-creep-controlled mantle impacts the planform of convection and the planetary tectonic regime as a function of the lithospheric yield strength in numerical models of mantle convection self-generating plate-like tectonics. The low upper-mantle viscosities caused by zones of substantial dislocation creep produce contrasting effects on surface dynamics. For strong lithosphere (yield strength >35 MPa), the large lithosphere-asthenosphere viscosity contrasts promote stagnant-lid convection. In contrast, the increase of upper mantle convective vigor enhances plate mobility for lithospheric strength <35 MPa. For the here-used model assumptions, composite rheology does not facilitate the onset of plate-like behavior at large lithospheric strength.

Plain Language Summary

Understanding uppermost mantle flow and deformation is important to study Earth's surface evolution, since plate tectonics and mantle convection are intertwined processes. Observations and experiments provide important - yet uncertain - constraints suggesting that uppermost mantle viscosity should be at least partially controlled by dislocation creep (i.e. its rheology should vary non-linearly with stress). However, most studies have not included dislocation creep. Here, we incorporate different amounts of this deformation mechanism in global-scale numerical models of mantle convection featuring Earth-like tectonic plates. We demonstrate that fast-evolving low-viscosity areas containing dislocation creep arise around slabs and plumes. Moreover, large amounts of dislocation creep alter surface tectonics in several ways: for a weak lithosphere, subductions become shorter-lived and plate velocities increase. For a strong lithosphere, in contrast, plate tectonics is inhibited. This study therefore demonstrates the key role of composite rheology in understanding mantle-lithosphere interactions.

1 Introduction

The lithospheric behavior of terrestrial bodies notably depends on their mantle properties and dynamics (e.g. Alisic et al., 2012; Coltice et al., 2017; Garel et al., 2020). In particular, mantle rheology determines the coupling between the convecting mantle and the lithosphere, therefore affecting surface heat transfer, plate velocities and continental motions (e.g. Stein et al., 2004; Rolf et al., 2018). Rock-deformation laboratory experiments conducted at upper-mantle conditions (Fig 1a-b, e.g. Hirth & Kohlstedt, 2003; Karato & Wu, 1993) show that mantle rheology is composite, meaning that deformation is driven by a coexistence of different creep mechanisms such as diffusion creep (linear or Newtonian stress/strain-rate dependence) and dislocation creep (non-linear power-law or non-Newtonian stress/strain-rate relationship). These experimental results are corroborated by the observed spatial heterogeneity in the strength of uppermost-mantle seismic anisotropy (e.g. Beghein et al., 2014; Debayle & Ricard, 2013), which could be at least partially explained by different amounts of olivine lattice preferred orientations (LPO), possibly caused by the heterogeneous development of dislocation creep in the uppermost mantle (e.g. Becker et al., 2006; Hedjazian et al., 2017; Nicolas & Christensen, 1987).

While mantle composite rheology is typically considered in regional-scale geodynamics models (e.g. Billen & Hirth, 2005; Garel et al., 2020; Neuharth & Mittelstaedt, 2023), it is often neglected in global-scale models (e.g. Coltice et al., 2017; Li & Zhong, 2019; Stein et al., 2004), or simply mimicked by reduced activation energy in pure diffusion creep rheology (Christensen, 1983, 1984). However, this latter approximation causes differences in the planform of stagnant-lid convection compared to using full composite rheology (e.g. Schulz et al., 2020). Moreover, prescribing pure diffusion creep makes it difficult to fully capture Earth's lithosphere and mantle behavior, such as observed plume swells' shapes (Asaadi et al., 2011), trench retreat rates (Holt & Becker, 2016), seismic anisotropy patterns around slabs (Jadamec & Billen, 2010), surface dynamic topography amplitudes (e.g. Bodur & Rey, 2019), and subduction geometry during its initiation (e.g. Billen & Hirth, 2005). Numerical studies prescribing pure dislocation creep in the upper-mantle have shown its importance for all these processes. However, in a composite formulation, the spatiotemporal distribution of the different creep mechanisms is not determined a priori, but arises self-consistently. Accounting for it therefore allows us to evaluate where substantial dislocation creep may occur in the mantle and to further study its effects on geodynamic processes. Some global models of mantle convection with plate-like behavior recently included composite rheology (e.g. Dannberg et al., 2017; Rozel, 2012), but these computationally-demanding models used a single set of rheological activation parameters based on experimental values, while estimates vary over a large range (e.g. Ranalli, 2001; Korenaga & Karato, 2008; Jain et al., 2018, 2019). Moreover, these numerical studies focussed on the effect of grain-size evolution on the planform of convection and on the lithospheric behavior. Therefore, a systematic exploration of the effects of composite rheology in the upper mantle is still needed.

Here, we explore how the temperature-, depth- and stress-dependent diffusion/dislocation creep partitioning impacts the planform of convection and the tectonic regime in 2D-cartesian whole-mantle convection models with composite rheology and static grain-size self-generating plate tectonics. Our goal is not to use Earth-like rheological parameters, but rather investigate the geodynamic effects of different parametrizations of composite rheology and capture qualitative convective and tectonic trends relevant for the Earth (Fig. 1). We find that composite rheology influences both mantle convective planform and surface tectonics due to its spatio-temporal dynamic effect on uppermost mantle viscosity, either enhancing or altering plate mobility and plateness depending on lithospheric strength. These results demonstrate that uncertainties in experimentally-determined rheological parameters lead to substantial geodynamical effects, and calls for further consideration of composite rheology in studies of mantle-lithosphere interactions.

2 Methods

2.1 On the use of composite rheology

Mantle viscosity varies with temperature (T), pressure (P), grain-size (d) and stress (σ) (e.g. Hirth & Kohlstedt, 2003; Karato & Wu, 1993):

$$\eta_{mech} = A_{mech} d^m \sigma^{1-n} \exp\left(\frac{E_{mech} + PV_{mech}}{RT}\right). \tag{1}$$

R is the gas constant, m is the grain-size exponent and n is the stress exponent. E_{mech}, V_{mech} and A_{mech} are respectively the activation energy, the activation volume and a pre-exponential factor (accounting for all other effects on mantle rheology, such as water and melt content) for the rheological mechanism ($mech$) considered (diffusion or dislocation creep).

Diffusion creep dominates below and dislocation creep dominates above the transition stress (σ_t) at which the strain-rates due to the two different mechanisms are equal ($\dot{\epsilon}_{diff} = \dot{\epsilon}_{disl}$, e.g. Christensen, 1984; Hall & Parmentier, 2003):

$$\sigma_t = \left(\frac{A_{diff}}{A_{disl}}\right)^{\frac{1}{n-1}} d^{-\frac{m}{n-1}} \exp\left(\frac{(E_{disl} - E_{diff}) + P(V_{disl} - V_{diff})}{RT}\right)^{\frac{1}{n-1}} . \quad (2)$$

E_{diff}, E_{disl}, V_{diff} and V_{disl} can be determined for olivine from rock experiments (e.g. Karato & Wu, 1993) and vary respectively between $240-450$ kJ/mol, $430-560$ kJ/mol, $0-20$ cm^3/mol and $0-33$ cm^3/mol (Hirth & Kohlstedt, 2003; Karato & Wu, 1993; Ranalli, 2001), depending on water content. Despite those uncertainties, $E_{diff} < E_{disl}$ and $V_{diff} < V_{disl}$ (Fig. 1a-b, e.g Karato & Wu, 1993). Those experiments predict that dislocation creep should dominate in hot regions of the uppermost-mantle and areas submitted to high stresses (Fig. 1a-b).

2.2 Numerical model setup

We solve the non-dimensional equations of mass, momentum and energy conservation under the Boussinesq approximation using StagYY (e.g. Tackley, 2000a) on a 2D-cartesian 512x128 or 768x192 grid (aspect ratio 4:1). Grid cells are refined near the thermal boundary layers. Top and bottom boundaries are free-slip, lateral boundaries are periodic. We use a reference Rayleigh number of 10^7. The mantle is heated both from below and from within (constant internal heating rate $H = 8.6 \times 10^{-12}$ W kg^{-1}, Table S1).

We use a pseudoplastic rheology to model plate-like behavior (e.g. Trompert & Hansen, 1998; Tackley, 2000a), and vary the surface yield stress σ_{Y_0}, which represents lithospheric strength, between 12 and 234 MPa. The yield stress varies with depth at a rate of ~ 0.3 MPa km^{-1}. The surface yield stress is bounded by the typical stress drop during earthquakes (10 MPa, Allmann & Shearer, 2009) and the yield stress of pristine lithospheric rocks measured in experiments (Brace & Kohlstedt, 1980). Over the modeled range of yield stresses, diverse tectonic behaviors are expected for pure diffusion creep: from mobile plates at low yield stress to stagnant-lid at high yield stress (e.g. Arnould et al., 2018).

In StagYY, the transition stress σ_t^* between diffusion and dislocation creep is defined in analogy to Eq. 2 as:

$$\sigma_t^* = \sigma_0 \left(\frac{B_{disl}}{B_{diff}}\right)^{\frac{1}{n-1}} \left(\frac{d}{d_0}\right)^{-\frac{m}{n-1}} \exp\left(\frac{(E_{disl} - E_{diff}) + P(V_{disl} - V_{diff})}{R(T + T_0 - T_{surf})}\right)^{\frac{1}{n-1}} . \quad (3)$$

$T_0 = 0.64$ is the non-dimensional reference temperature, equivalent to 1,600 K and $T_{surf} = 0.12$ is the non-dimensional surface temperature, equivalent to 300 K. σ_0 is a reference transition stress. B_{diff} and B_{disl} differ from A_{mech} in Eq. 1 and ensure that mantle viscosity equals the non-dimensional reference viscosity $\eta_0 = 1$ (9.8×10^{21} Pa s) at reference conditions (temperature of 1,600 K and surface pressure). As we do not account for grain-size evolution, $d = d_0$ unless explicitly mentioned otherwise (see Discussion in section 4). For dislocation creep, m=0 and n=3.5 while for diffusion creep, m=2 and n=1.

2.3 Computed cases

For each value of σ_{Y_0}, we fix E_{diff}, V_{diff}, and E_{disl}, but vary V_{disl} by a factor of $\sim$3, since its experimental value is subjected to the largest uncertainties (e.g. Karato & Wu, 1993; Korenaga & Karato, 2008). We also vary σ_0 between 1.2 and 3.5 MPa to ensure that dislocation creep is mostly restricted to the upper mantle. We choose lower activation parameters than experimentally determined for pristine olivine for reasons of numerical feasibility. Instead, we preserve ranges of variation for $E_{disl} - E_{diff}$ and $V_{disl} - V_{diff}$ similar to rock experiments (Karato and Wu (1993), Fig. 1) since these differences matter the most in Eq. 2 and 3. The spatio-temporal evolution of mantle convection self-consistently partitions the mantle into areas dominated by dislocation creep or diffusion creep, depending on the value of stress.

For each yield stress, we first ran models in pure diffusion creep over 3 Gyr, starting from a stratified thermal field with small perturbations to initiate convection. We then restarted from the final thermal field of these models while including composite rheology and ran those new models over 3 Gyr. Since we do not model evolutionary models, this procedure ensures that the models are in quasi-statistical steady-state (Fig. S2) during the last 400 Myr of each simulation that we analyse. Detailed model parameters, with their non-dimensional and dimensional values are given in Table S1.

3 Results

3.1 Spatio-temporal distribution of dislocation creep

Decreasing both V_{disl} and/or σ_0 results in a thicker and more continuous layer deforming in dislocation creep in the upper mantle (Fig. 2). As a consequence, upper man-

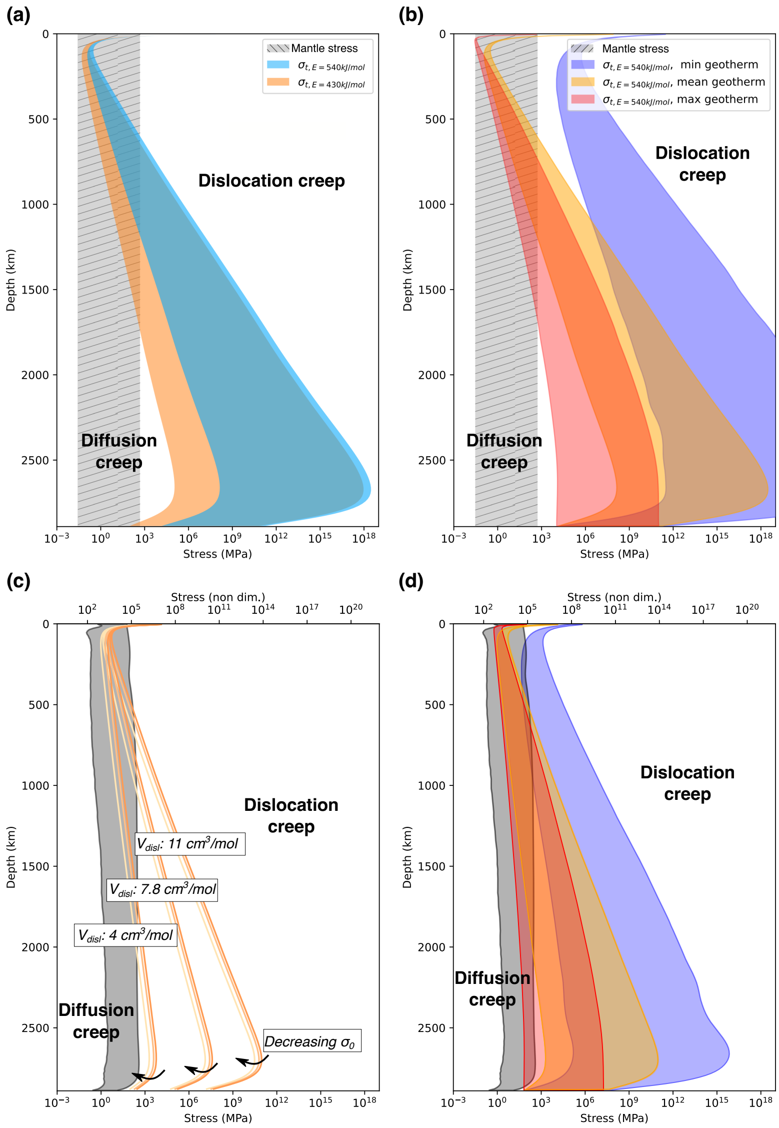

Figure 1. Top: Range of olivine transition stress measured by Karato and Wu (1993), assuming a grain-size of 1 mm. (a) Sensitivity to E_{disl} (blue: 430 kJ mol^{-1}, orange: 540 kJ mol^{-1}) and V_{disl} (10-25 cm^3 mol^{-1}), using an average geotherm from a reference model in pure diffusion creep (Fig. S1e). (b) Sensitivity to temperature using E_{disl} = 430 kJ mol^{-1} and $10 < V_{disl} < 25$ cm^3 mol^{-1} (blue=cold, yellow=average, and red=hot geotherm (Fig. S1e)). **Bottom:** Same as above, but for our modeling setup. (c) Sensitivity of the model transition stress to V_{disl} (4-11 cm^3 mol^{-1}) and σ_0 (1.2-3.5 MPa), using an average geotherm (Fig. S1e). (d) Sensitivity to temperature. In all panels, gray-striped areas show the stress rage expected in Earth's mantle (top) and predicted in our reference model (bottom, Fig. S1b).

tle viscosity decreases by at least one order of magnitude on average. Moreover, average horizontal and vertical velocities increase by a factor of 3 depending on the amount of dislocation creep (Fig. 2a), irrespective of the surface yield stress (Fig. S3), showing that composite rheology enhances convective vigor locally. Due to its location and low viscosity signature, the layer containing >10% dislocation creep is here-after referred to as an "asthenosphere" in models with composite rheology, although it sometimes locally reaches lower-mantle depths (low V_{disl} and σ_0).

Areas strongly affected by dislocation creep show a high spatio-temporal variability within the asthenospheric layer (Fig. 2b-d and Supplementary Movie 1), which produces large lateral viscosity variations in the upper mantle, as shown by e.g. Alisic et al. (2012); Billen and Hirth (2007); Semple and Lenardic (2020). In models featuring plate-like behavior, dislocation creep mainly occurs around slabs and plumes in the uppermost mantle. Indeed, ambient mantle shearing by sinking slabs is responsible for the highest convective stresses, and thus for a higher proportion of dislocation creep around them. In contrast and depending on their thickness, slab interiors deform mostly through diffusion creep (Fig. 2b-c) because of their much colder state (Fig. 1b and d). The evolution of individual slabs is significantly affected by composite rheology, consistent with regional thermo-mechanical models (e.g. Garel et al., 2020): slabs tend to sink faster through an upper mantle with more abundant dislocation creep and thus a more pronounced low viscosity zone (Fig. 2). Moreover, they tend to buckle and/or break-off more easily depending on their strength and the mantle viscosity structure (Fig. 4a and d). In fact, both the amount of dislocation creep around slabs and the thickness of the asthenosphere are responsible for creating a viscosity contrast between the upper and the lower mantle, which hinders the sinking of slabs and affects their evolution (Fig. 2a, e.g Billen and Hirth (2007)).

Around plumes, hot mantle more likely deforms through dislocation creep (Fig. 1b and d), although shearing is less important than around slabs. Plumes are thus also surrounded by lower viscosities than pure diffusion creep cases, which favors fast rising (Fig. 2 and Fig. S4). Plume material further tends to feed fast lateral asthenospheric channeled-flow (as proposed by e.g. Phipps Morgan et al., 1995) in which dislocation creep occurs more likely due to high temperatures and stresses, favoring even lower viscosity in these areas than in diffusion creep models (Fig. 2a and b). This occurs preferentially when new plume heads reach sub-lithospheric depths. Over a few million to a few tens of million

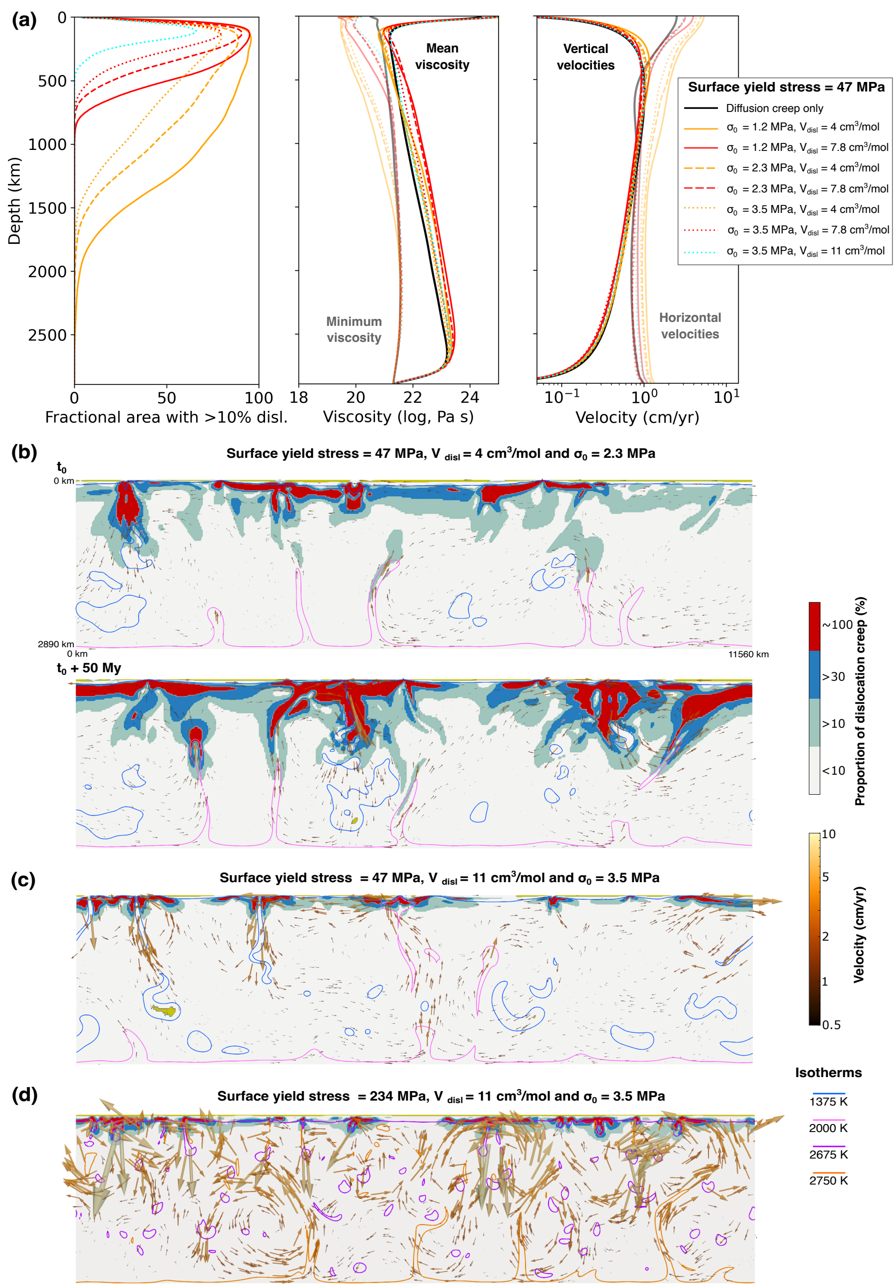

Figure 2. (a) Time-averaged profiles of (left) mantle fractional area with >10 % dislocation creep, (middle) minimum and mean viscosity, and (right) vertical and horizontal velocity for models with a surface yield stress σ_{Y_0} = 47 MPa. (b-d) Proportion of dislocation creep and mantle velocity field (arrows scaled and coloured by magnitude) in three models. In (b), a 50 Myr-evolution is shown. In (b-c), blue lines show slabs and magenta lines contour plumes. In (d), purple lines contour dripping lithosphere and orange lines show hotter-than-average upwellings.

years, the geometry and abundance of dislocation creep can therefore vary considerably (Fig. 2b and c), controlled by the dynamics of convective thermal heterogeneities.

Models with surface yield strength larger than 120 MPa experience stagnant-lid convection. In these models, the mantle is much warmer due to limited heat loss, thus favoring more vigorous and smaller-scale convection than in cases with plate-like behavior (Fig. 2). Higher temperature and increased convective vigor promote dislocation creep, which emerges in areas of basal lithosphere dripping, or around hotter-than-average upwellings in the shallow mantle (Fig. 2c). The large variability of these processes controls the spatio-temporal distribution of dislocation creep.

3.2 Effects on the tectonic regime

The effect of composite rheology on the surface tectonic regime is quantified through surface mobility $M = \frac{v_{surf}}{v_{rms}}$ (with v_{surf} the average surface velocity and v_{rms} the volume root-mean-square velocity) and plateness $P = 1 - \frac{\mathrm{def}_{90}}{\mathrm{def}_{90,iso}}$ (with def_{90} being the fractional surface area containing 90% of deformation, and $\mathrm{def}_{90,iso}$ being the value for an isoviscous model, Tackley, 2000a). These proxies are close to 1 for the mobile-lid regime and tend to 0 in the stagnant-lid regime, with episodic transitioning between these end-members. In addition, we track the number of active subduction zones, detected from surface downward velocity peaks, and the lithospheric thickness, defined from the inflection point of the time-averaged temperature profile (Fig. 3 and Fig. S5).

Regardless of the surface yield strength, lithosphere thickness decreases as the proportion of dislocation creep increases (Fig. 3a and Fig. S5), by up to 60% compared to diffusion creep models. In the asthenospheric areas strongly affected by dislocation creep, increased convective vigor tends to impede lithospheric growth due to more efficient convective erosion. Therefore, the thicker the layer with substantial dislocation creep, the thinner is the lithosphere for a given surface yield stress compared to pure diffusion-creep models. Besides the major control of surface lithospheric yield strength, composite rheology has two contrasting effects on the tectonic regime. These effects are summarized on Fig. 4a-c and described below.

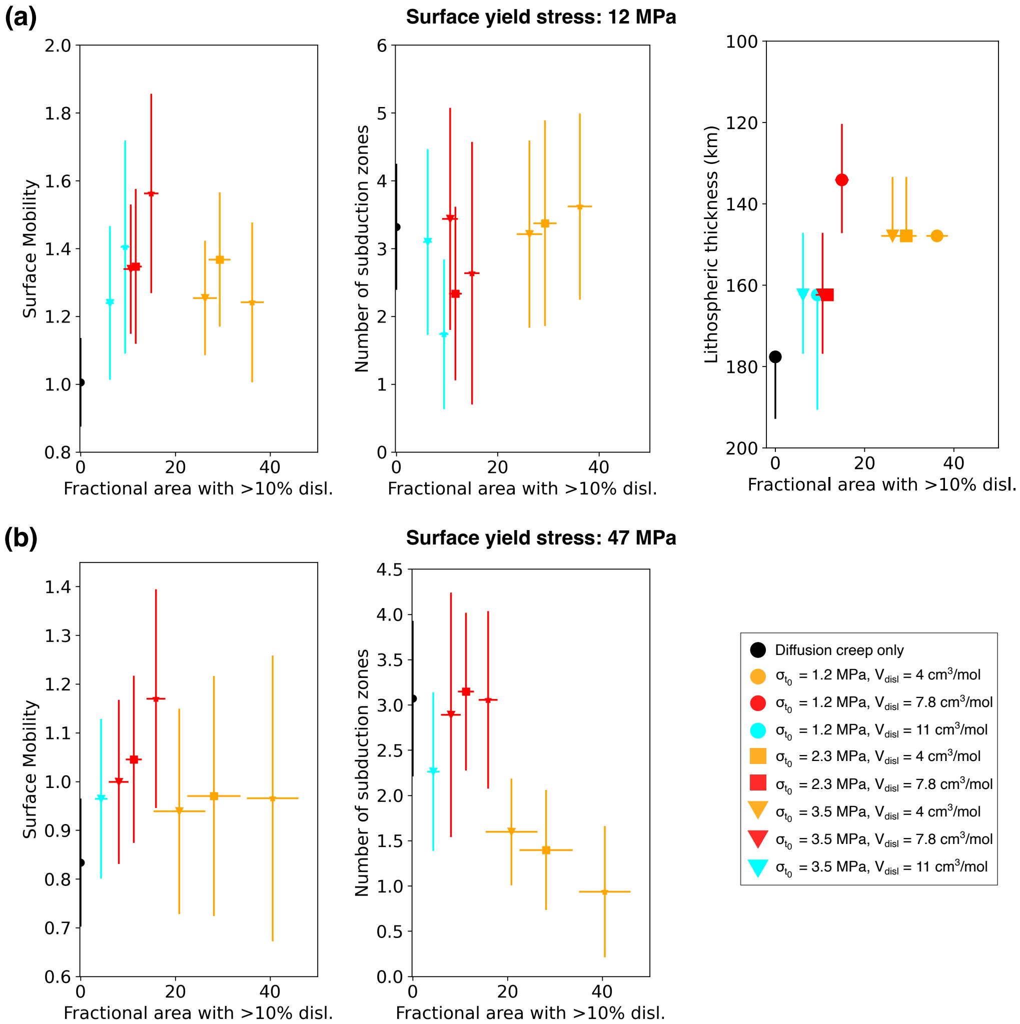

Figure 3. Effect of composite rheology on surface tectonic regime (temporal average and standard deviation of surface mobility, number of subduction zones and lithosphere thickness as a function of the time-averaged mantle fractional area containing >10% dislocation creep) in models with $\sigma_{Y_0} = 12$ MPa (a) and 47 MPa (b).

3.2.1 Models with a weak lithosphere (<35 MPa)

For yield stresses below ∼35 MPa, models in pure diffusion creep are in the mobile-lid regime. Composite rheology enhances surface mobility (up to 1.6) and plateness. Active subduction zones tend to be shorter-lived (Fig. 4d). In these models, the viscosity reduction in the uppermost mantle induced by dislocation creep leads to the decoupling of lithosphere from the asthenosphere via lubrication, and to reduced stress acting on the lithosphere although local convective vigor increases (Tackley, 2000b). This decou-

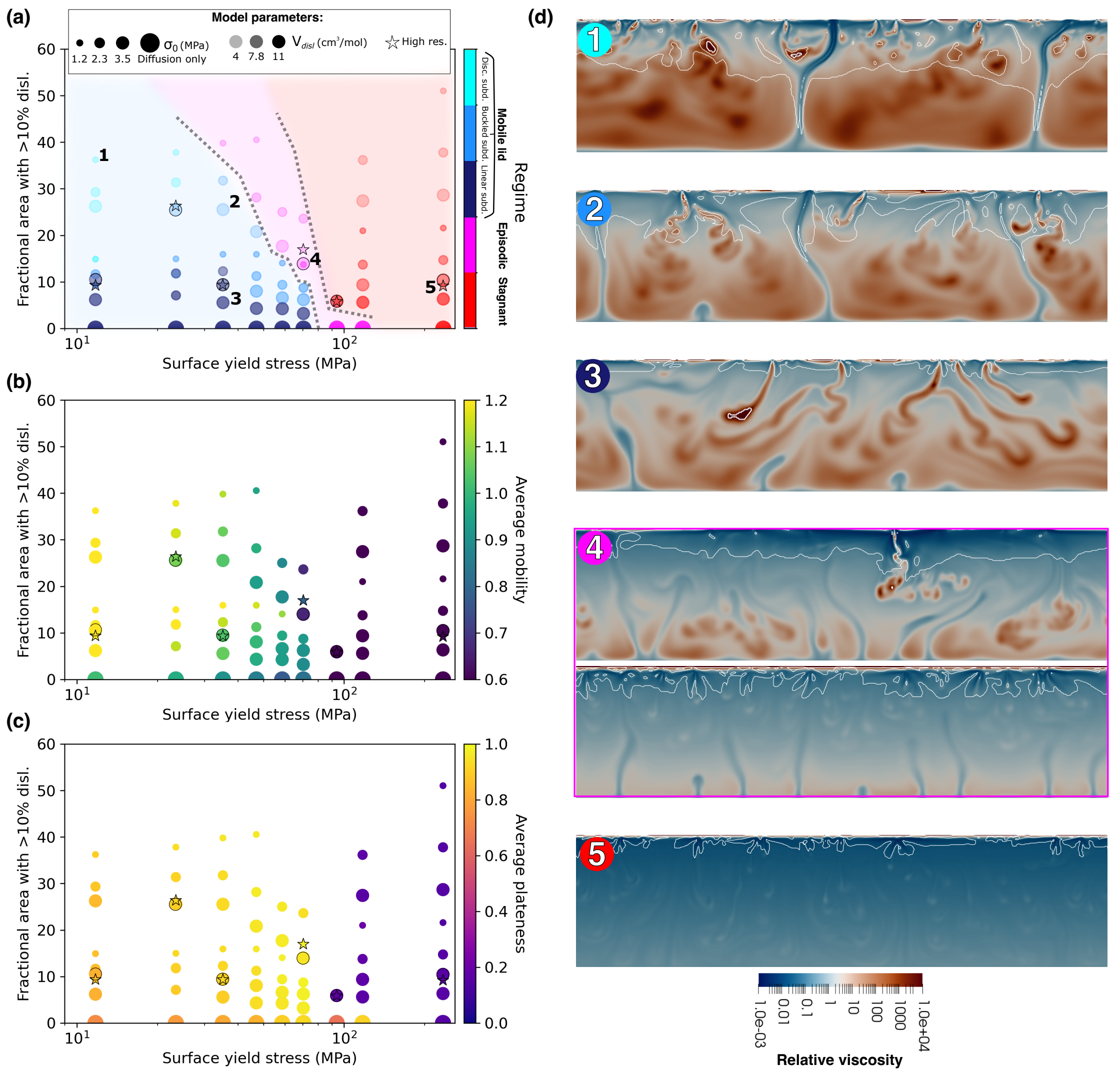

Figure 4. (a) Regime diagram of all models. Mobile-lid models have discontinuous and short-lived subductions (cyan), buckled slabs (blue), or mostly linear slabs (deep-blue). Episodic models (magenta) have intermediate plateness and mobility. Stagnant-lid models (red) have low plateness and mobility. Qualitative boundaries are drawn between each regime. (b-c) Similar to (a) but with colours representing time-averaged surface mobility and plateness, respectively. (d) Snapshots of viscosity of selected models referred as numbers in (a). White lines contour low-viscosity regions with >10% dislocation creep.

pling contributes to the observed increase in mobility. Since dislocation creep also favors lithosphere thinning, the plastic strength at lithospheric base is reduced compared to models in pure diffusion creep. Therefore, an increasing amount of dislocation creep enhances thin slab break-offs. Accounting for composite rheology in models with a low lithospheric strength thus enhances mobile-lid convection.

3.2.2 Models with a strong lithosphere (>35 MPa)

Models in pure diffusion creep with surface yield stresses comprised between ~35 MPa and ~120 MPa are also still in the mobile-lid regime. Including composite rheology with decreasing values of V_{disl} and/or σ_0 results in up to 40 % of the mantle being affected by dislocation creep (Fig. 3b and 4a-c).

For small amounts of dislocation creep in the mantle (<20%), both plateness and surface mobility tend to increase by a factor of up to 1.4 and the number of slabs remains stable (Fig. 3b). In these models, thin low-viscosity asthenospheric areas tend to lubricate the base of the lithosphere, enhancing plate mobility and plateness (e.g. Tackley, 2000b).

When the proportion of dislocation creep exceeds 20%, the number of active subductions, plateness, and surface mobility decrease (Fig. 3b, 4a-c, and S5b). Lithosphere-asthenosphere decoupling promotes episodic and stagnant-lid convection (Fig. 4). This strengthening phenomenon due to large viscosity contrasts between the convecting mantle and the lithosphere has long been demonstrated using Newtonian rheology (e.g. Moresi & Solomatov, 1995; Solomatov, 1995; Höink et al., 2012, although the latter study invoked a flow channelization effect as being responsible for stagnant-lid convection) and non-Newtonian rheology in the asthenosphere (Semple & Lenardic, 2020, although they did not employ temperature- and depth-dependent viscosity, in contrast to the present study).

We further tested higher surface yield stresses (>120 MPa), which led to continuous stagnant-lid behavior irrespective of our choice of activation parameters. Like in models with a lower yield stress, decreasing V_{disl} and/or σ_0 produces a thickening of the layer containing dislocation creep. Although the convective regime remains unchanged in these models, changing the amount of dislocation creep can strongly decrease the viscosity in the asthenosphere and decrease lithospheric thickness by up to 60%. These effects could have a large impact on the distribution of partial melting and the rates of magmatism on stagnant-lid planets (e.g. Schulz et al., 2020; Tosi & Padovan, 2021). However, these models also suggest that once a stagnant-lid is established with a pure diffusion creep rheology, adding composite rheology in the upper-mantle does not promote the generation of more plate-like behavior.

4 Discussion and conclusion

4.1 Model assumptions

Model setup simplifications potentially alter mantle flow and therefore the spatio-temporal diffusion/dislocation creep partitioning. Our models are limited to 2D-cartesian, have a reference Rayleigh number ∼10 times lower than Earth's, lower lithospheric strengths than inferred from laboratory experiments (e.g. Brace & Kohlstedt, 1980), and lower activation parameters for olivine than those predicted by rock experiments (e.g. Hirth & Kohlstedt, 2003). We do not consider multiple mantle and lithosphere compositions and phases (e.g. King, 2016). We also only tested one initial thermal state for our models with composite rheology although different initial conditions could lead to distinct regime boundaries for diffusion-creep-only and composite rheology, as shown in e.g. Semple and Lenardic (2021); Weller and Lenardic (2018).

However, our mobile-lid models still produce mantle velocities of the order of the cm/yr (Fig. 2a), oceanic lithosphere thickness of 100-200 km, and successfully generate dislocation creep where it is expected to occur from rock-deformation experiments (Fig. 1). We also note no significant difference when increasing the resolution (Fig. 4a-c, star symbols). Therefore, we anticipate that the general convective and tectonic trends (Fig. 4) and physical mechanisms described in this study still apply using more Earth-like setups. In particular, we obtain a self-generated and self-evolving low-viscosity asthenosphere without invoking water and/or partial melting (King, 2016; Semple & Lenardic, 2020), the latter being often called on to justify the use of weakening laws to improve plateness in whole-mantle Newtonian models (e.g. Tackley, 2000a; Bello et al., 2015).

Importantly, we assumed a uniform static grain-size, although rock-deformation experiments indicate that diffusion creep should strongly depend on grain-size evolution (Eq. 1). In some stagnant-lid models, we increased the static grain size, which produced an increase in mantle average viscosity, stress, and proportion of dislocation creep in the uppermost mantle (Fig. S6), associated with lithospheric thickening, as already described in Schulz et al. (2020). This test, applied to models without dynamic grain-growth and reduction, reveals the competing effects of large grain size (which tends to increase mantle viscosity) and large amounts of dislocation creep (which tend to decrease it) on lithosphere thickness, at least up to a doubling of static grain-size with our setup (Fig. S6). Further exploring the role of grain-size evolution in mobile-lid scenarios is therefore needed to further understand the role of composite rheology on mantle and lithosphere dynamics.

4.2 Earth's observations and composite rheology in the uppermost mantle

On Earth, seismic anisotropy, through the generation of dislocation creep-induced LPO (e.g. Nicolas & Christensen, 1987), can provide complementary insight on the lateral variations of mantle rheological properties (e.g. Becker et al., 2008). Although 3D modeling is required to quantitatively compare the diffusion/dislocation creep partitioning in our models with observed seismic anisotropy, our results already potentially explain its observed orientation and strength variations (e.g. Debayle et al., 2005), as well as high strength around slabs (e.g. Jadamec & Billen, 2012) and in the thermal trail of plumes (e.g. Barruol et al., 2019). The correlation between strong anisotropy and fast plate velocities described in Debayle and Ricard (2013) could also partly result from the fact that these plates are attached to fast sinking slabs, thus favoring more dislocation creep due to lithosphere basal shear. One future direction would therefore be to estimate seismic anisotropy in more Earth-like models with composite rheology and compare it to Earth's observations (e.g. Kendall et al., 2022). Together with the consideration that some rheological parameters are inter-dependent (e.g. Jain et al., 2019), this should provide complementary constraints on the range of rheological parameters applicable to Earth. Finally, another independent constraint could come from the study of how composite rheology affects the spatio-temporal distribution of surface dynamic topography, both on the long-term (e.g. Bodur & Rey, 2019) and on shorter glacial-isostatic-adjustment timescales (Kang et al., 2022).

In this study, we show that our choice of composite rheological parameters impacts uppermost mantle spatio-temporal viscosity variations and dynamics, therefore affecting convection and surface tectonics in a non-linear way: at low lithospheric strength, increasing the proportion of mantle deforming through dislocation creep promotes plate mobility as well as numerous, weaker and short-lived slabs. In contrast, increasing the proportion of mantle containing dislocation creep in models with large lithospheric strength, results in episodic to stagnant-lid convection. This shows the potential geodynamical influence of experimental uncertainties of the rheological parameters and calls for both further experimental refinement of mantle rheological parameters such as V_{disl}, and further exploration of the effects of composite rheology on mantle convective planform and surface tectonics in more sophisticated planetary-scale models.

Open Research

The convection code StagYY (Tackley, 2008) is property of ETH Zurich and Paul J. Tackley. Data files used in this study can be downloaded from Arnould (2022).

Acknowledgments

This research benefited from Norwegian Research Council funding to the Centre for Earth Evolution and Dynamics (223272) and to TR (PLATONICS, 276032). MA benefited from INSU-PNP and UCBL-BQR fundings. Computations were performed on Stallo and Saga Uninett Sigma2 facilities (nn9010k, ns9010k). Crameri et al. (2020) authored Fig.4d colormap.

References

Alisic, L., Gurnis, M., Stadler, G., Burstedde, C., & Ghattas, O. (2012). Multi-scale dynamics and rheology of mantle flow with plates. *Journal of Geophysical Research: Solid Earth*, *117*(B10), 148–227. doi: https://doi.org/10.1029/2012JB009234

Allmann, B. P., & Shearer, P. M. (2009). Global variations of stress drop for moderate to large earthquakes. *Journal of Geophysical Research: Solid Earth*, *114*(B1).

Arnould, M. (2022, Apr). *Effects of composite rheology on plate-like behaviour in global-scale mantle convection [dataset].* OSF. Retrieved from `osf.io/p3mvn`

Arnould, M., Coltice, N., Flament, N., Seigneur, V., & Muller, R. D. (2018). On the scales of dynamic topography in whole-mantle convection models. *Geochemistry, Geophysics, Geosystems*, *19*(9), 3140-3163.

Asaadi, N., Ribe, N. M., & Sobouti, F. (2011). Inferring nonlinear mantle rheology from the shape of the hawaiian swell. *Nature*, *473*(7348), 501–504.

Barruol, G., Sigloch, K., Scholz, J.-R., Mazzullo, A., Stutzmann, E., Montagner, J.-P., ... others (2019). Large-scale flow of indian ocean asthenosphere driven by réunion plume. *Nature Geoscience*, *12*(12), 1043–1049.

Becker, T. W., Chevrot, S., Schulte-Pelkum, V., & Blackman, D. K. (2006). Statistical properties of seismic anisotropy predicted by upper mantle geodynamic models. *Journal of Geophysical Research: Solid Earth*, *111*(B8).

Becker, T. W., Kustowski, B., & Ekström, G. (2008). Radial seismic anisotropy as a constraint for upper mantle rheology. *Earth and Planetary Science Letters*, *267*(1-2), 213–227.

Beghein, C., Yuan, K., Schmerr, N., & Xing, Z. (2014). Changes in seismic anisotropy shed light on the nature of the gutenberg discontinuity. *Science*, *343*(6176), 1237–1240.

Bello, L., Coltice, N., Tackley, P. J., Müller, R. D., & Cannon, J. (2015). Assessing the role of slab rheology in coupled plate-mantle convection models. *Earth and Planetary Science Letters*, *430*, 191–201.

Billen, M. I., & Hirth, G. (2005). Newtonian versus non-newtonian upper mantle viscosity: Implications for subduction initiation. *Geophysical Research Letters*, *32*(19). doi: https://doi.org/10.1029/2005GL023457

Billen, M. I., & Hirth, G. (2007). Rheologic controls on slab dynamics. *Geochemistry, Geophysics, Geosystems*, *8*(8). doi: https://doi.org/10.1029/2007GC001597

Bodur, Ö. F., & Rey, P. F. (2019). The impact of rheological uncertainty on dynamic topography predictions. *Solid Earth*, *10*(6), 2167–2167.

Brace, W. F., & Kohlstedt, D. L. (1980). Limits on lithospheric stress imposed by laboratory experiments. *Journal of Geophysical Research: Solid Earth*, *85*(B11), 6248-6252. Retrieved from `https://agupubs.onlinelibrary.wiley.com/doi/abs/10.1029/JB085iB11p06248` doi: https://doi.org/10.1029/JB085iB11p06248

Christensen, U. (1983). Convection in a variable-viscosity fluid: Newtonian versus power-law rheology. *Earth and Planetary Science Letters*, *64*(1), 153–162.

Christensen, U. (1984). Convection with pressure-and temperature-dependent non-newtonian rheology. *Geophysical Journal International*, *77*(2), 343–384.

Coltice, N., Gérault, M., & Ulvrová, M. (2017). A mantle convection perspective on global tectonics. *Earth-science reviews*, *165*, 120–150.

Crameri, F., Shephard, G. E., & Heron, P. J. (2020). The misuse of colour in science communication. *Nature communications*, *11*(1), 1–10.

Dannberg, J., Eilon, Z., Faul, U., Gassmöller, R., Moulik, P., & Myhill, R. (2017). The importance of grain size to mantle dynamics and seismological observations. *Geochemistry, Geophysics, Geosystems*, *18*(8), 3034–3061.

Debayle, E., Kennett, B., & Priestley, K. (2005). Global azimuthal seismic anisotropy and the unique plate-motion deformation of australia. *Nature*, *433*(7025), 509–512.

Debayle, E., & Ricard, Y. (2013). Seismic observations of large-scale deformation at the bottom of fast-moving plates. *Earth and Planetary Science Letters*, *376*, 165–177.

Garel, F., Thoraval, C., Tommasi, A., Demouchy, S., & Davies, D. R. (2020). Using thermo-mechanical models of subduction to constrain effective mantle viscosity. *Earth and Planetary Science Letters*, *539*, 116243. doi: https://doi.org/10.1016/j.epsl.2020.116243

Hall, C. E., & Parmentier, E. (2003). Influence of grain size evolution on convective instability. *Geochemistry, Geophysics, Geosystems*, *4*(3). doi: https://doi.org/10.1029/2002GC000308

Hedjazian, N., Garel, F., Davies, D. R., & Kaminski, E. (2017). Age-independent seismic anisotropy under oceanic plates explained by strain history in the asthenosphere. *Earth and Planetary Science Letters*, *460*, 135–142.

Hirth, G., & Kohlstedt, D. (2003). Rheology of the upper mantle and the mantle wedge: A view from the experimentalists. *Geophysical Monograph-American Geophysical Union*, *138*, 83–106.

Höink, T., Lenardic, A., & Richards, M. (2012). Depth-dependent viscosity and mantle stress amplification: implications for the role of the asthenosphere in maintaining plate tectonics. *Geophysical Journal International*, *191*(1), 30–41.

Holt, A. F., & Becker, T. W. (2016). The effect of a power-law mantle viscosity on trench retreat rate. *Geophysical Journal International*, 491–507.

Jadamec, M., & Billen, M. (2010). Reconciling surface plate motions with rapid three-dimensional mantle flow around a slab edge. *Nature*, *465*(7296), 338–341.

Jadamec, M., & Billen, M. I. (2012). The role of rheology and slab shape on rapid mantle flow: Three-dimensional numerical models of the alaska slab edge. *Journal of Geophysical Research: Solid Earth*, *117*(B2). doi: https://doi.org/10.1029/2011JB008563

Jain, C., Korenaga, J., & Karato, S.-i. (2018). On the grain size sensitivity of olivine rheology. *Journal of Geophysical Research: Solid Earth*, *123*(1), 674–688.

Jain, C., Korenaga, J., & Karato, S.-i. (2019). Global analysis of experimental data on the rheology of olivine aggregates. *Journal of Geophysical Research: Solid Earth*, *124*(1), 310–334.

Kang, K., Zhong, S., Geruo, A., & Mao, W. (2022). The effects of non-newtonian rheology in the upper mantle on relative sea level change and geodetic observables induced by glacial isostatic adjustment process. *Geophysical Journal International*, *228*(3), 1887–1906.

Karato, S.-i., & Wu, P. (1993). Rheology of the upper mantle: A synthesis. *Science*, *260*(5109), 771–778.

Kendall, E., Faccenda, M., Ferreira, A., & Chang, S.-J. (2022). On the relationship between oceanic plate speed, tectonic stress, and seismic anisotropy. *Geophysical Research Letters*, *49*(15), e2022GL097795.

King, S. D. (2016). An evolving view of transition zone and midmantle viscosity. *Geochemistry, Geophysics, Geosystems*, *17*(3), 1234–1237.

Korenaga, J., & Karato, S.-I. (2008). A new analysis of experimental data on olivine rheology. *Journal of Geophysical Research: Solid Earth*, *113*(B2).

Li, M., & Zhong, S. (2019). Lateral motion of mantle plumes in 3-d geodynamic models. *Geophysical Research Letters*, *46*(9), 4685–4693.

Moresi, L.-N., & Solomatov, V. (1995). Numerical investigation of 2d convection with extremely large viscosity variations. *Physics of Fluids*, *7*(9), 2154–2162.

Neuharth, D., & Mittelstaedt, E. (2023). Temporal variations in plume flux: characterizing pulsations from tilted plume conduits in a rheologically complex mantle. *Geophysical Journal International*, *233*(1), 338–358.

Nicolas, A., & Christensen, N. I. (1987). Formation of anisotropy in upper mantle peridotites-a review. *Composition, structure and dynamics of the lithosphere-asthenosphere system*, *16*, 111–123.

Phipps Morgan, J., Morgan, W. J., Zhang, Y.-S., & Smith, W. H. (1995). Observational hints for a plume-fed, suboceanic asthenosphere and its role in mantle convection. *Journal of Geophysical Research: Solid Earth*, *100*(B7), 12753–12767.

Ranalli, G. (2001). Mantle rheology: radial and lateral viscosity variations inferred from microphysical creep laws. *Journal of Geodynamics*, *32*(4-5), 425–444.

Rolf, T., Capitanio, F. A., & Tackley, P. J. (2018). Constraints on mantle viscosity structure from continental drift histories in spherical mantle convection models. *Tectonophysics*, *746*, 339–351.

Rozel, A. (2012). Impact of grain size on the convection of terrestrial planets. *Geochemistry, Geophysics, Geosystems*, *13*(10). doi: https://doi.org/10.1029/2012GC004282

Schulz, F., Tosi, N., Plesa, A.-C., & Breuer, D. (2020). Stagnant-lid convection with diffusion and dislocation creep rheology: Influence of a non-evolving grain size. *Geophysical Journal International*, *220*(1), 18–36.

Semple, A., & Lenardic, A. (2020). The robustness of pressure-driven asthenospheric flow in mantle convection models with plate-like behavior. *Geophysical Research Letters*, *47*(17), e2020GL089556.

Semple, A., & Lenardic, A. (2021). Feedbacks between a non-newtonian upper mantle, mantle viscosity structure and mantle dynamics. *Geophysical Journal International*, *224*(2), 961–972.

Solomatov, V. (1995). Scaling of temperature-and stress-dependent viscosity convection. *Physics of Fluids*, *7*(2), 266–274.

Stein, C., Schmalzl, J., & Hansen, U. (2004). The effect of rheological parameters on plate behaviour in a self-consistent model of mantle convection. *Physics of the Earth and Planetary Interiors*, *142*(3-4), 225–255.

Tackley, P. J. (2000a). Self-consistent generation of tectonic plates in time-dependent, three-dimensional mantle convection simulations. *Geochemistry, Geophysics, Geosystems*, *1*(8). doi: https://doi.org/10.1029/2000GC000036

Tackley, P. J. (2000b). Self-consistent generation of tectonic plates in time-dependent, three-dimensional mantle convection simulations 2. strain weakening and asthenosphere. *Geochemistry, Geophysics, Geosystems*, *1*(8). doi: https://doi.org/10.1029/2000GC000043

Tackley, P. J. (2008). Modelling compressible mantle convection with large viscosity contrasts in a three-dimensional spherical shell using the yin-yang grid. *Physics* *of the Earth and Planetary Interiors*, *171*(1-4), 7–18. doi: https://doi.org/10.1016/j.pepi.2008.08.005

Tosi, N., & Padovan, S. (2021). Mercury, moon, mars. In *Mantle convection and surface expressions* (p. 455-489). American Geophysical Union (AGU). Retrieved from https://agupubs.onlinelibrary.wiley.com/doi/abs/10.1002/9781119528609.ch17 doi: https://doi.org/10.1002/9781119528609.ch17

Trompert, R., & Hansen, U. (1998). Mantle convection simulations with rheologies that generate plate-like behaviour. *Nature*, *395*(6703), 686–689.

Weller, M. B., & Lenardic, A. (2018). On the evolution of terrestrial planets: Bi-stability, stochastic effects, and the non-uniqueness of tectonic states. *Geoscience Frontiers*, *9*(1), 91–102.

Figure 1.

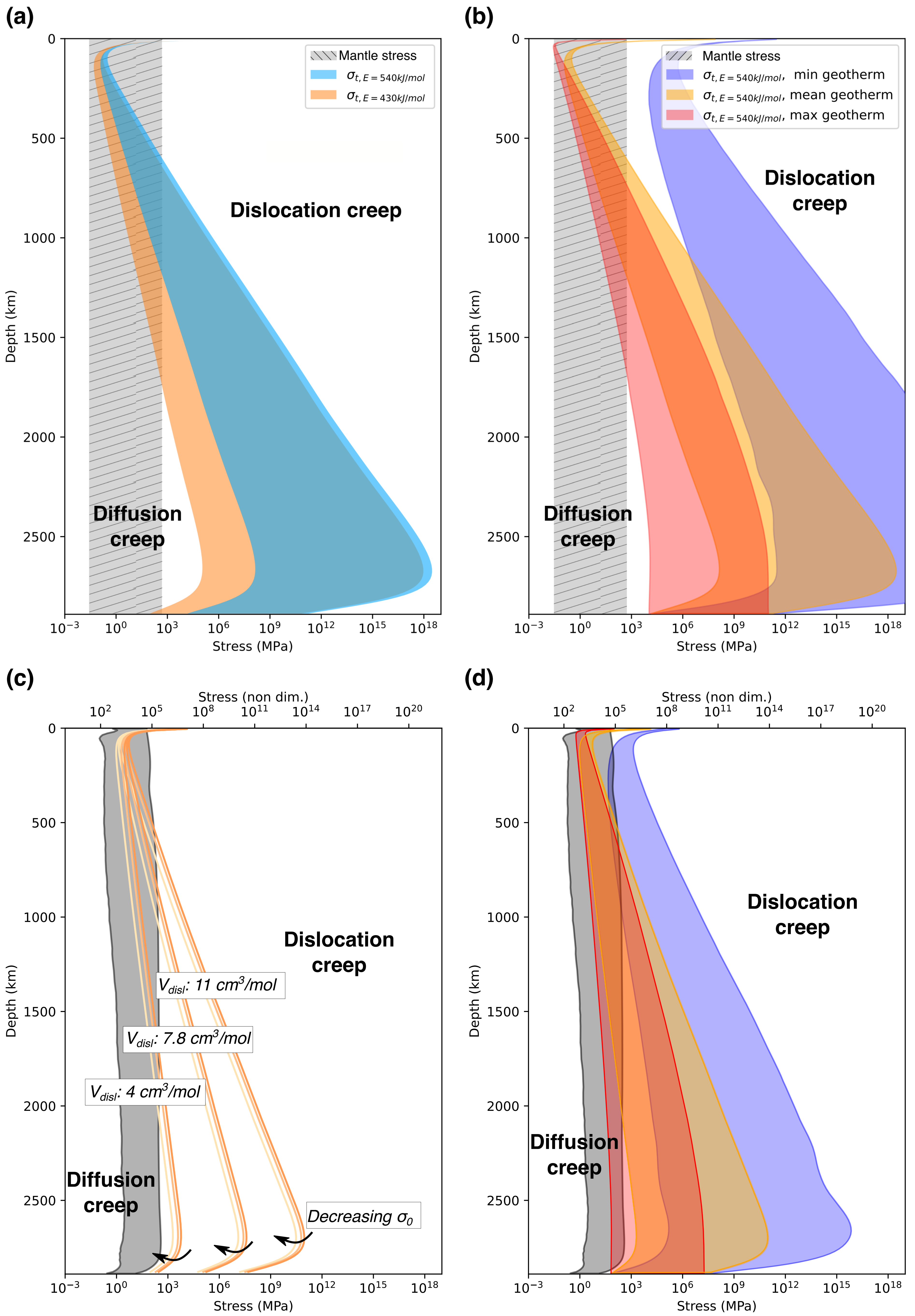

(a)
(b)
(c)
(d)
Mantle stress
$\sigma_{t,E=540kJ/mol}$
$\sigma_{t,E=430kJ/mol}$
$\sigma_{t,E=540kJ/mol}$, min geotherm
$\sigma_{t,E=540kJ/mol}$, mean geotherm
$\sigma_{t,E=540kJ/mol}$, max geotherm
Dislocation creep
Diffusion creep
Depth (km)
Stress (MPa)
Stress (non dim.)
V_{disl}: 11 cm^3/mol
V_{disl}: 7.8 cm^3/mol
V_{disl}: 4 cm^3/mol
Decreasing σ_0

Figure 2.


(a)
Depth (km)
Fractional area with >10% disl.
Mean viscosity
Minimum viscosity
Viscosity (log, Pa s)
Vertical velocities
Horizontal velocities
Velocity (cm/yr)
Surface yield stress = 47 MPa
Diffusion creep only
σ_0 = 1.2 MPa, V_{disl} = 4 cm^3/mol
σ_0 = 1.2 MPa, V_{disl} = 7.8 cm^3/mol
σ_0 = 2.3 MPa, V_{disl} = 4 cm^3/mol
σ_0 = 2.3 MPa, V_{disl} = 7.8 cm^3/mol
σ_0 = 3.5 MPa, V_{disl} = 4 cm^3/mol
σ_0 = 3.5 MPa, V_{disl} = 7.8 cm^3/mol
σ_0 = 3.5 MPa, V_{disl} = 11 cm^3/mol
(b)
Surface yield stress = 47 MPa, V_{disl} = 4 cm^3/mol and σ_0 = 2.3 MPa
t_0
0 km
2890 km
0 km
11560 km
t_0 + 50 My
(c)
Surface yield stress = 47 MPa, V_{disl} = 11 cm^3/mol and σ_0 = 3.5 MPa
(d)
Surface yield stress = 234 MPa, V_{disl} = 11 cm^3/mol and σ_0 = 3.5 MPa
Proportion of dislocation creep (%)
~100
>30
>10
<10
Velocity (cm/yr)
Isotherms
1375 K
2000 K
2675 K
2750 K

Figure 3.

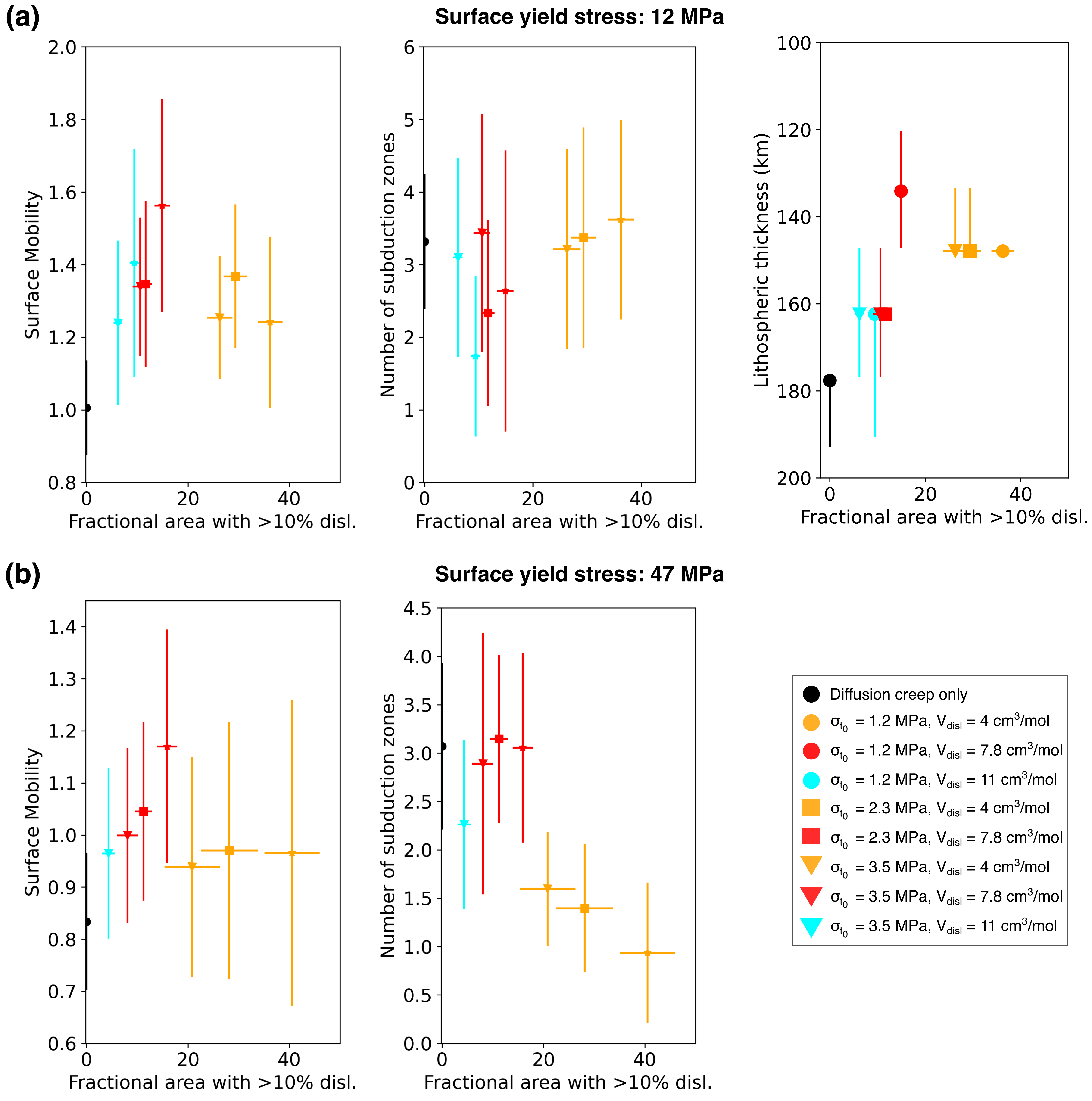

(a)
Surface yield stress: 12 MPa
Surface Mobility
Number of subduction zones
Lithospheric thickness (km)
Fractional area with >10% disl.
(b)
Surface yield stress: 47 MPa
Surface Mobility
Number of subduction zones
Fractional area with >10% disl.
Diffusion creep only
σ_{t_0} = 1.2 MPa, V_{disl} = 4 cm^3/mol
σ_{t_0} = 1.2 MPa, V_{disl} = 7.8 cm^3/mol
σ_{t_0} = 1.2 MPa, V_{disl} = 11 cm^3/mol
σ_{t_0} = 2.3 MPa, V_{disl} = 4 cm^3/mol
σ_{t_0} = 2.3 MPa, V_{disl} = 7.8 cm^3/mol
σ_{t_0} = 3.5 MPa, V_{disl} = 4 cm^3/mol
σ_{t_0} = 3.5 MPa, V_{disl} = 7.8 cm^3/mol
σ_{t_0} = 3.5 MPa, V_{disl} = 11 cm^3/mol

Figure 4.

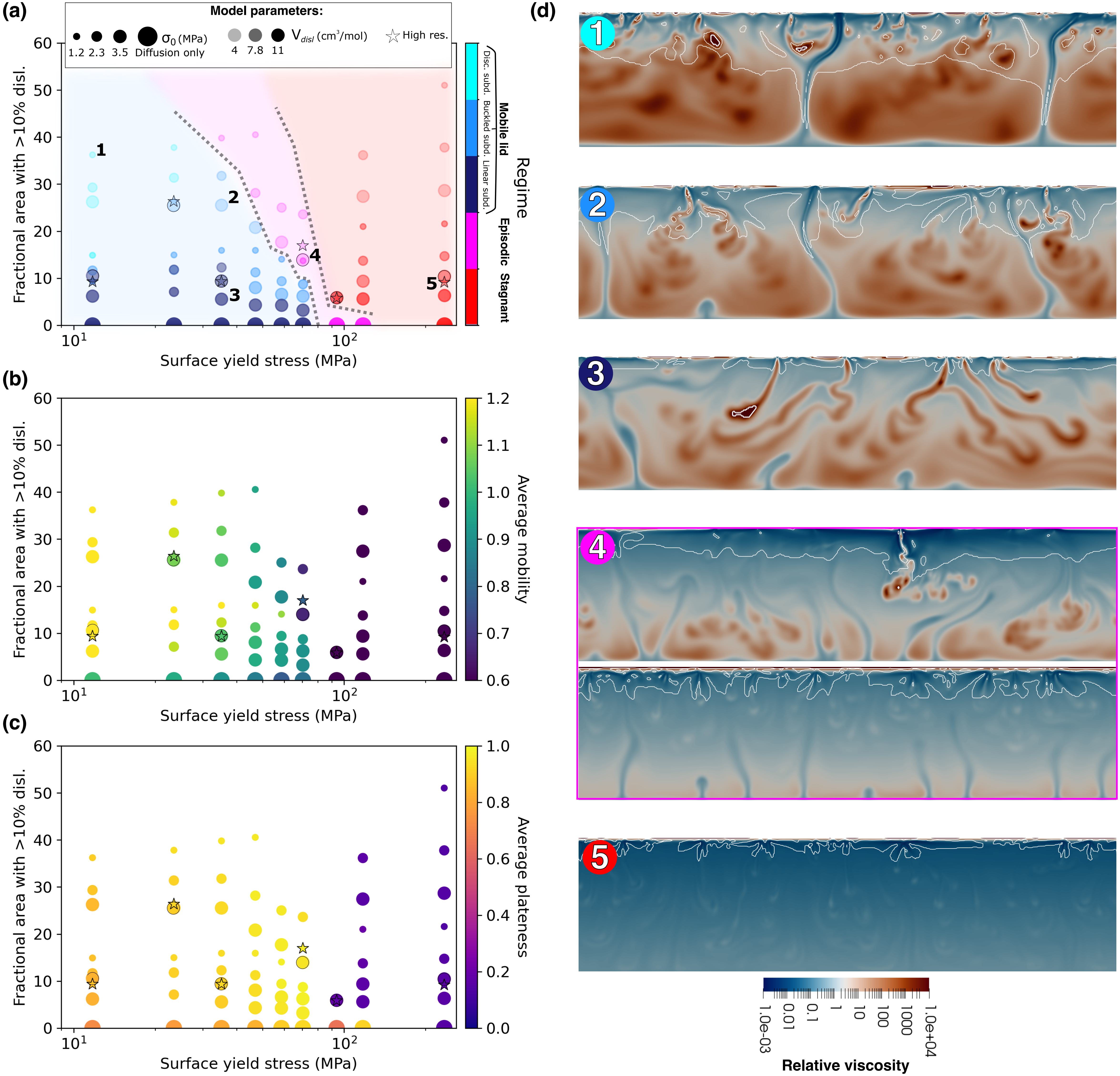

(a)
Model parameters:
1.2 2.3 3.5 Diffusion only
σ0 (MPa)
4 7.8 11
V_disl (cm³/mol)
High res.
Fractional area with >10% disl.
Surface yield stress (MPa)
Regime
Mobile lid
Disc. subd.
Buckled subd.
Linear subd.
Episodic
Stagnant
(b)
Average mobility
(c)
Average plateness
(d)
Relative viscosity
1.0e-03 0.01 0.1 1 10 100 1000 1.0e+04

Effects of composite rheology on plate-like behavior in global-scale mantle convection

Maëlis Arnould [1,2], Tobias Rolf [2,3] and Antonio Manjón-Cabeza Córdoba [2,4,5]

[1]University of Lyon, UCBL, ENSL, UJM, CNRS 5276, Laboratoire de Géologie de Lyon - Terre, Planètes, Environnement, Lyon, France

[2]Centre for Earth Evolution and Dynamics, Department of Geosciences, University of Oslo, Blindern, Oslo, Norway

[3]Institute of Geophysics, University of Münster, Germany

[4]Andalusian Earth Sciences Institute, University of Grenada, Spain

[5]Department of Earth Sciences, University College London, UK

Key Points:

- Uppermost mantle viscosity variations induced by composite rheology control surface tectonics
- Composite rheology can impede or enhance plate mobility depending on lithospheric strength
- Composite rheology does not facilitate the onset of subduction for large yield stress

Corresponding author: Maelis Arnould, `maelis.arnould@univ-lyon1.fr`

Abstract

Earth's upper mantle rheology controls lithosphere-asthenosphere coupling and thus surface tectonics. Rock deformation experiments and seismic anisotropy measurements indicate that composite rheology (co-existing diffusion and dislocation creep) occurs in the Earth's uppermost mantle, potentially affecting convection and surface tectonics. Here, we investigate how the spatio-temporal distribution of dislocation creep in an otherwise diffusion-creep-controlled mantle impacts the planform of convection and the planetary tectonic regime as a function of the lithospheric yield strength in numerical models of mantle convection self-generating plate-like tectonics. The low upper-mantle viscosities caused by zones of substantial dislocation creep produce contrasting effects on surface dynamics. For strong lithosphere (yield strength >35 MPa), the large lithosphere-asthenosphere viscosity contrasts promote stagnant-lid convection. In contrast, the increase of upper mantle convective vigor enhances plate mobility for lithospheric strength <35 MPa. For the here-used model assumptions, composite rheology does not facilitate the onset of plate-like behavior at large lithospheric strength.

Plain Language Summary

Understanding uppermost mantle flow and deformation is important to study Earth's surface evolution, since plate tectonics and mantle convection are intertwined processes. Observations and experiments provide important - yet uncertain - constraints suggesting that uppermost mantle viscosity should be at least partially controlled by dislocation creep (i.e. its rheology should vary non-linearly with stress). However, most studies have not included dislocation creep. Here, we incorporate different amounts of this deformation mechanism in global-scale numerical models of mantle convection featuring Earth-like tectonic plates. We demonstrate that fast-evolving low-viscosity areas containing dislocation creep arise around slabs and plumes. Moreover, large amounts of dislocation creep alter surface tectonics in several ways: for a weak lithosphere, subductions become shorter-lived and plate velocities increase. For a strong lithosphere, in contrast, plate tectonics is inhibited. This study therefore demonstrates the key role of composite rheology in understanding mantle-lithosphere interactions.

1 Introduction

The lithospheric behavior of terrestrial bodies notably depends on their mantle properties and dynamics (e.g. Alisic et al., 2012; Coltice et al., 2017; Garel et al., 2020). In particular, mantle rheology determines the coupling between the convecting mantle and the lithosphere, therefore affecting surface heat transfer, plate velocities and continental motions (e.g. Stein et al., 2004; Rolf et al., 2018). Rock-deformation laboratory experiments conducted at upper-mantle conditions (Fig 1a-b, e.g. Hirth & Kohlstedt, 2003; Karato & Wu, 1993) show that mantle rheology is composite, meaning that deformation is driven by a coexistence of different creep mechanisms such as diffusion creep (linear or Newtonian stress/strain-rate dependence) and dislocation creep (non-linear power-law or non-Newtonian stress/strain-rate relationship). These experimental results are corroborated by the observed spatial heterogeneity in the strength of uppermost-mantle seismic anisotropy (e.g. Beghein et al., 2014; Debayle & Ricard, 2013), which could be at least partially explained by different amounts of olivine lattice preferred orientations (LPO), possibly caused by the heterogeneous development of dislocation creep in the uppermost mantle (e.g. Becker et al., 2006; Hedjazian et al., 2017; Nicolas & Christensen, 1987).

While mantle composite rheology is typically considered in regional-scale geodynamics models (e.g. Billen & Hirth, 2005; Garel et al., 2020; Neuharth & Mittelstaedt, 2023), it is often neglected in global-scale models (e.g. Coltice et al., 2017; Li & Zhong, 2019; Stein et al., 2004), or simply mimicked by reduced activation energy in pure diffusion creep rheology (Christensen, 1983, 1984). However, this latter approximation causes differences in the planform of stagnant-lid convection compared to using full composite rheology (e.g. Schulz et al., 2020). Moreover, prescribing pure diffusion creep makes it difficult to fully capture Earth's lithosphere and mantle behavior, such as observed plume swells' shapes (Asaadi et al., 2011), trench retreat rates (Holt & Becker, 2016), seismic anisotropy patterns around slabs (Jadamec & Billen, 2010), surface dynamic topography amplitudes (e.g. Bodur & Rey, 2019), and subduction geometry during its initiation (e.g. Billen & Hirth, 2005). Numerical studies prescribing pure dislocation creep in the upper-mantle have shown its importance for all these processes. However, in a composite formulation, the spatiotemporal distribution of the different creep mechanisms is not determined a priori, but arises self-consistently. Accounting for it therefore allows us to evaluate where substantial dislocation creep may occur in the mantle and to further study its effects on geodynamic processes. Some global models of mantle convection with plate-like behavior recently included composite rheology (e.g. Dannberg et al., 2017; Rozel, 2012), but these computationally-demanding models used a single set of rheological activation parameters based on experimental values, while estimates vary over a large range (e.g. Ranalli, 2001; Korenaga & Karato, 2008; Jain et al., 2018, 2019). Moreover, these numerical studies focussed on the effect of grain-size evolution on the planform of convection and on the lithospheric behavior. Therefore, a systematic exploration of the effects of composite rheology in the upper mantle is still needed.

Here, we explore how the temperature-, depth- and stress-dependent diffusion/dislocation creep partitioning impacts the planform of convection and the tectonic regime in 2D-cartesian whole-mantle convection models with composite rheology and static grain-size self-generating plate tectonics. Our goal is not to use Earth-like rheological parameters, but rather investigate the geodynamic effects of different parametrizations of composite rheology and capture qualitative convective and tectonic trends relevant for the Earth (Fig. 1). We find that composite rheology influences both mantle convective planform and surface tectonics due to its spatio-temporal dynamic effect on uppermost mantle viscosity, either enhancing or altering plate mobility and plateness depending on lithospheric strength. These results demonstrate that uncertainties in experimentally-determined rheological parameters lead to substantial geodynamical effects, and calls for further consideration of composite rheology in studies of mantle-lithosphere interactions.

2 Methods

2.1 On the use of composite rheology

Mantle viscosity varies with temperature (T), pressure (P), grain-size (d) and stress (σ) (e.g. Hirth & Kohlstedt, 2003; Karato & Wu, 1993):

$$\eta_{mech} = A_{mech} d^m \sigma^{1-n} \exp\left(\frac{E_{mech} + PV_{mech}}{RT}\right). \tag{1}$$

R is the gas constant, m is the grain-size exponent and n is the stress exponent. E_{mech}, V_{mech} and A_{mech} are respectively the activation energy, the activation volume and a pre-exponential factor (accounting for all other effects on mantle rheology, such as water and melt content) for the rheological mechanism ($mech$) considered (diffusion or dislocation creep).

Diffusion creep dominates below and dislocation creep dominates above the transition stress (σ_t) at which the strain-rates due to the two different mechanisms are equal ($\dot{\epsilon}_{diff} = \dot{\epsilon}_{disl}$, e.g. Christensen, 1984; Hall & Parmentier, 2003):

$$\sigma_t = \left(\frac{A_{diff}}{A_{disl}}\right)^{\frac{1}{n-1}} d^{-\frac{m}{n-1}} \exp\left(\frac{(E_{disl} - E_{diff}) + P(V_{disl} - V_{diff})}{RT}\right)^{\frac{1}{n-1}} . \tag{2}$$

E_{diff}, E_{disl}, V_{diff} and V_{disl} can be determined for olivine from rock experiments (e.g. Karato & Wu, 1993) and vary respectively between $240-450$ kJ/mol, $430-560$ kJ/mol, $0-20$ cm^3/mol and $0-33$ cm^3/mol (Hirth & Kohlstedt, 2003; Karato & Wu, 1993; Ranalli, 2001), depending on water content. Despite those uncertainties, $E_{diff} < E_{disl}$ and $V_{diff} < V_{disl}$ (Fig. 1a-b, e.g Karato & Wu, 1993). Those experiments predict that dislocation creep should dominate in hot regions of the uppermost-mantle and areas submitted to high stresses (Fig. 1a-b).

2.2 Numerical model setup

We solve the non-dimensional equations of mass, momentum and energy conservation under the Boussinesq approximation using StagYY (e.g. Tackley, 2000a) on a 2D-cartesian 512x128 or 768x192 grid (aspect ratio 4:1). Grid cells are refined near the thermal boundary layers. Top and bottom boundaries are free-slip, lateral boundaries are periodic. We use a reference Rayleigh number of 10^7. The mantle is heated both from below and from within (constant internal heating rate $H = 8.6 \times 10^{-12}$ W kg^{-1}, Table S1).

We use a pseudoplastic rheology to model plate-like behavior (e.g. Trompert & Hansen, 1998; Tackley, 2000a), and vary the surface yield stress σ_{Y_0}, which represents lithospheric strength, between 12 and 234 MPa. The yield stress varies with depth at a rate of ~ 0.3 MPa km^{-1}. The surface yield stress is bounded by the typical stress drop during earthquakes (10 MPa, Allmann & Shearer, 2009) and the yield stress of pristine lithospheric rocks measured in experiments (Brace & Kohlstedt, 1980). Over the modeled range of yield stresses, diverse tectonic behaviors are expected for pure diffusion creep: from mobile plates at low yield stress to stagnant-lid at high yield stress (e.g. Arnould et al., 2018).

In StagYY, the transition stress σ_t^* between diffusion and dislocation creep is defined in analogy to Eq. 2 as:

$$\sigma_t^* = \sigma_0 \left(\frac{B_{disl}}{B_{diff}}\right)^{\frac{1}{n-1}} \left(\frac{d}{d_0}\right)^{-\frac{m}{n-1}} \exp\left(\frac{(E_{disl} - E_{diff}) + P(V_{disl} - V_{diff})}{R(T + T_0 - T_{surf})}\right)^{\frac{1}{n-1}} . \tag{3}$$

$T_0 = 0.64$ is the non-dimensional reference temperature, equivalent to 1,600 K and $T_{surf} = 0.12$ is the non-dimensional surface temperature, equivalent to 300 K. σ_0 is a reference transition stress. B_{diff} and B_{disl} differ from A_{mech} in Eq. 1 and ensure that mantle viscosity equals the non-dimensional reference viscosity $\eta_0 = 1$ (9.8×10^{21} Pa s) at reference conditions (temperature of 1,600 K and surface pressure). As we do not account for grain-size evolution, $d = d_0$ unless explicitly mentioned otherwise (see Discussion in section 4). For dislocation creep, m=0 and n=3.5 while for diffusion creep, m=2 and n=1.

2.3 Computed cases

For each value of σ_{Y_0}, we fix E_{diff}, V_{diff}, and E_{disl}, but vary V_{disl} by a factor of $\sim$3, since its experimental value is subjected to the largest uncertainties (e.g. Karato & Wu, 1993; Korenaga & Karato, 2008). We also vary σ_0 between 1.2 and 3.5 MPa to ensure that dislocation creep is mostly restricted to the upper mantle. We choose lower activation parameters than experimentally determined for pristine olivine for reasons of numerical feasibility. Instead, we preserve ranges of variation for $E_{disl}-E_{diff}$ and $V_{disl}-V_{diff}$ similar to rock experiments (Karato and Wu (1993), Fig. 1) since these differences matter the most in Eq. 2 and 3. The spatio-temporal evolution of mantle convection self-consistently partitions the mantle into areas dominated by dislocation creep or diffusion creep, depending on the value of stress.

For each yield stress, we first ran models in pure diffusion creep over 3 Gyr, starting from a stratified thermal field with small perturbations to initiate convection. We then restarted from the final thermal field of these models while including composite rheology and ran those new models over 3 Gyr. Since we do not model evolutionary models, this procedure ensures that the models are in quasi-statistical steady-state (Fig. S2) during the last 400 Myr of each simulation that we analyse. Detailed model parameters, with their non-dimensional and dimensional values are given in Table S1.

3 Results

3.1 Spatio-temporal distribution of dislocation creep

Decreasing both V_{disl} and/or σ_0 results in a thicker and more continuous layer deforming in dislocation creep in the upper mantle (Fig. 2). As a consequence, upper man-

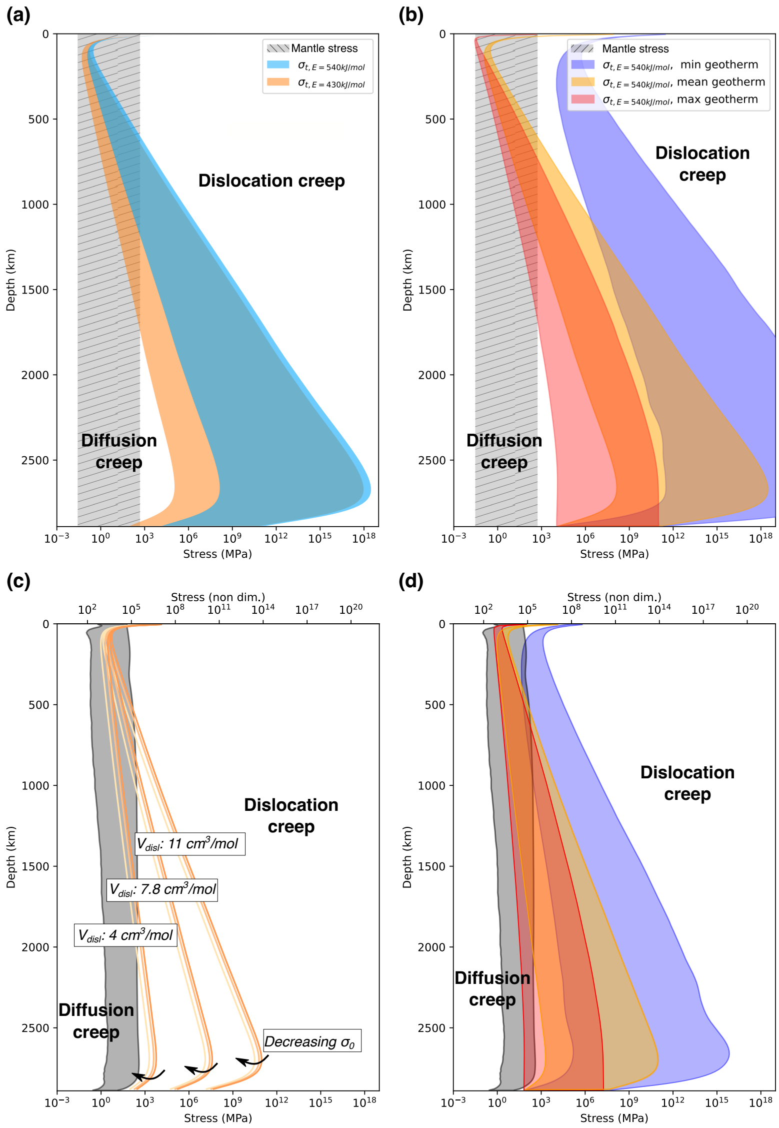

Figure 1. **Top:** Range of olivine transition stress measured by Karato and Wu (1993), assuming a grain-size of 1 mm. (a) Sensitivity to E_{disl} (blue: 430 kJ mol^{-1}, orange: 540 kJ mol^{-1}) and V_{disl} (10-25 cm^3 mol^{-1}), using an average geotherm from a reference model in pure diffusion creep (Fig. S1e). (b) Sensitivity to temperature using E_{disl} = 430 kJ mol^{-1} and $10 < V_{disl} < 25$ cm^3 mol^{-1} (blue=cold, yellow=average, and red=hot geotherm (Fig. S1e)). **Bottom:** Same as above, but for our modeling setup. (c) Sensitivity of the model transition stress to V_{disl} (4-11 cm^3 mol^{-1}) and σ_0 (1.2-3.5 MPa), using an average geotherm (Fig. S1e). (d) Sensitivity to temperature. In all panels, gray-striped areas show the stress rage expected in Earth's mantle (top) and predicted in our reference model (bottom, Fig. S1b).

tle viscosity decreases by at least one order of magnitude on average. Moreover, average horizontal and vertical velocities increase by a factor of 3 depending on the amount of dislocation creep (Fig. 2a), irrespective of the surface yield stress (Fig. S3), showing that composite rheology enhances convective vigor locally. Due to its location and low viscosity signature, the layer containing >10% dislocation creep is here-after referred to as an "asthenosphere" in models with composite rheology, although it sometimes locally reaches lower-mantle depths (low V_{disl} and σ_0).

Areas strongly affected by dislocation creep show a high spatio-temporal variability within the asthenospheric layer (Fig. 2b-d and Supplementary Movie 1), which produces large lateral viscosity variations in the upper mantle, as shown by e.g. Alisic et al. (2012); Billen and Hirth (2007); Semple and Lenardic (2020). In models featuring plate-like behavior, dislocation creep mainly occurs around slabs and plumes in the uppermost mantle. Indeed, ambient mantle shearing by sinking slabs is responsible for the highest convective stresses, and thus for a higher proportion of dislocation creep around them. In contrast and depending on their thickness, slab interiors deform mostly through diffusion creep (Fig. 2b-c) because of their much colder state (Fig. 1b and d). The evolution of individual slabs is significantly affected by composite rheology, consistent with regional thermo-mechanical models (e.g. Garel et al., 2020): slabs tend to sink faster through an upper mantle with more abundant dislocation creep and thus a more pronounced low viscosity zone (Fig. 2). Moreover, they tend to buckle and/or break-off more easily depending on their strength and the mantle viscosity structure (Fig. 4a and d). In fact, both the amount of dislocation creep around slabs and the thickness of the asthenosphere are responsible for creating a viscosity contrast between the upper and the lower mantle, which hinders the sinking of slabs and affects their evolution (Fig. 2a, e.g Billen and Hirth (2007)).

Around plumes, hot mantle more likely deforms through dislocation creep (Fig. 1b and d), although shearing is less important than around slabs. Plumes are thus also surrounded by lower viscosities than pure diffusion creep cases, which favors fast rising (Fig. 2 and Fig. S4). Plume material further tends to feed fast lateral asthenospheric channeled-flow (as proposed by e.g. Phipps Morgan et al., 1995) in which dislocation creep occurs more likely due to high temperatures and stresses, favoring even lower viscosity in these areas than in diffusion creep models (Fig. 2a and b). This occurs preferentially when new plume heads reach sub-lithospheric depths. Over a few million to a few tens of million

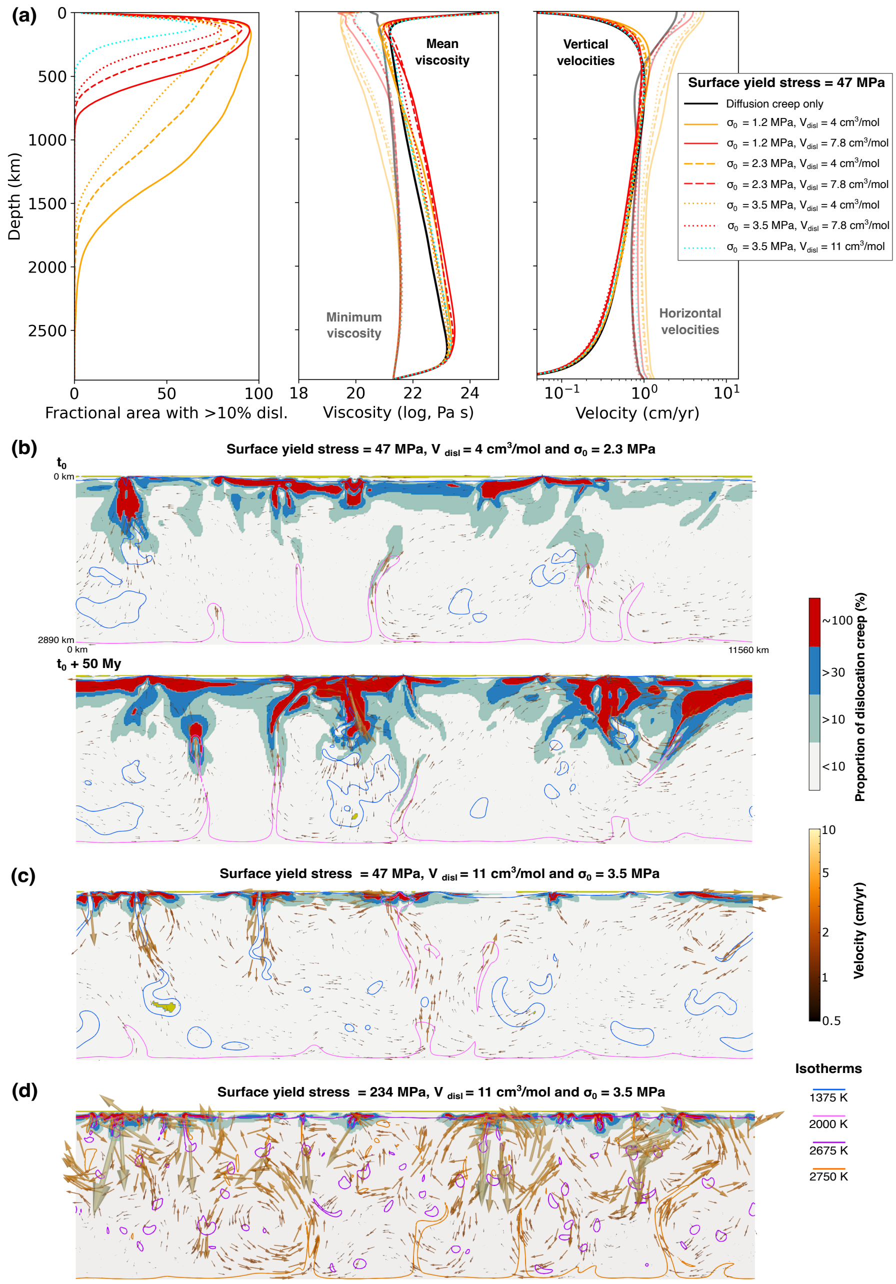

Figure 2. (a) Time-averaged profiles of (left) mantle fractional area with >10 % dislocation creep, (middle) minimum and mean viscosity, and (right) vertical and horizontal velocity for models with a surface yield stress σ_{Y_0} = 47 MPa. (b-d) Proportion of dislocation creep and mantle velocity field (arrows scaled and coloured by magnitude) in three models. In (b), a 50 Myr-evolution is shown. In (b-c), blue lines show slabs and magenta lines contour plumes. In (d), purple lines contour dripping lithosphere and orange lines show hotter-than-average upwellings.

years, the geometry and abundance of dislocation creep can therefore vary considerably (Fig. 2b and c), controlled by the dynamics of convective thermal heterogeneities.

Models with surface yield strength larger than 120 MPa experience stagnant-lid convection. In these models, the mantle is much warmer due to limited heat loss, thus favoring more vigorous and smaller-scale convection than in cases with plate-like behavior (Fig. 2). Higher temperature and increased convective vigor promote dislocation creep, which emerges in areas of basal lithosphere dripping, or around hotter-than-average upwellings in the shallow mantle (Fig. 2c). The large variability of these processes controls the spatio-temporal distribution of dislocation creep.

3.2 Effects on the tectonic regime

The effect of composite rheology on the surface tectonic regime is quantified through surface mobility $M = \frac{v_{surf}}{v_{rms}}$ (with v_{surf} the average surface velocity and v_{rms} the volume root-mean-square velocity) and plateness $P = 1 - \frac{\mathrm{def}_{90}}{\mathrm{def}_{90,iso}}$ (with def_{90} being the fractional surface area containing 90% of deformation, and $\mathrm{def}_{90,iso}$ being the value for an isoviscous model, Tackley, 2000a). These proxies are close to 1 for the mobile-lid regime and tend to 0 in the stagnant-lid regime, with episodic transitioning between these end-members. In addition, we track the number of active subduction zones, detected from surface downward velocity peaks, and the lithospheric thickness, defined from the inflection point of the time-averaged temperature profile (Fig. 3 and Fig. S5).

Regardless of the surface yield strength, lithosphere thickness decreases as the proportion of dislocation creep increases (Fig. 3a and Fig. S5), by up to 60% compared to diffusion creep models. In the asthenospheric areas strongly affected by dislocation creep, increased convective vigor tends to impede lithospheric growth due to more efficient convective erosion. Therefore, the thicker the layer with substantial dislocation creep, the thinner is the lithosphere for a given surface yield stress compared to pure diffusion-creep models. Besides the major control of surface lithospheric yield strength, composite rheology has two contrasting effects on the tectonic regime. These effects are summarized on Fig. 4a-c and described below.

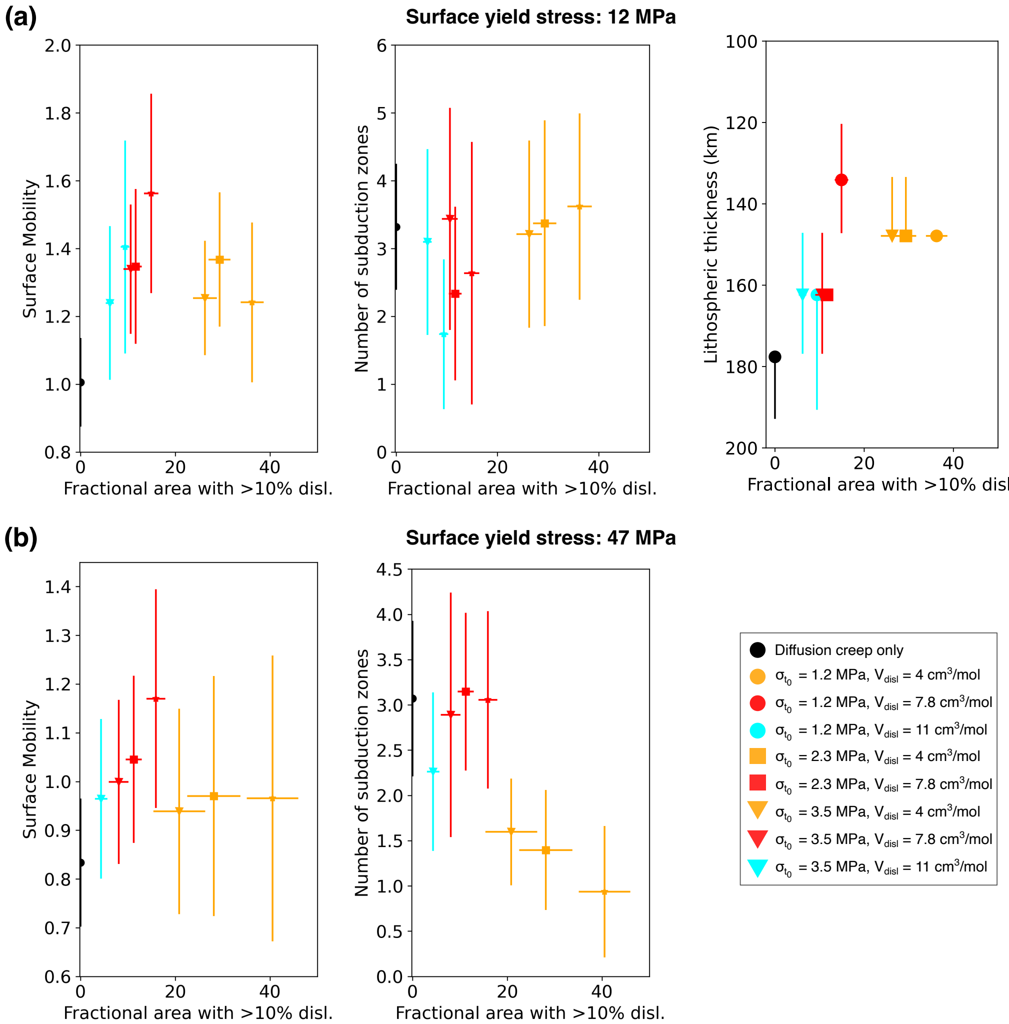

Figure 3. Effect of composite rheology on surface tectonic regime (temporal average and standard deviation of surface mobility, number of subduction zones and lithosphere thickness as a function of the time-averaged mantle fractional area containing >10% dislocation creep) in models with σ_{Y_0} = 12 MPa (a) and 47 MPa (b).

3.2.1 Models with a weak lithosphere (<35 MPa)

For yield stresses below ∼35 MPa, models in pure diffusion creep are in the mobile-lid regime. Composite rheology enhances surface mobility (up to 1.6) and plateness. Active subduction zones tend to be shorter-lived (Fig. 4d). In these models, the viscosity reduction in the uppermost mantle induced by dislocation creep leads to the decoupling of lithosphere from the asthenosphere via lubrication, and to reduced stress acting on the lithosphere although local convective vigor increases (Tackley, 2000b). This decou-

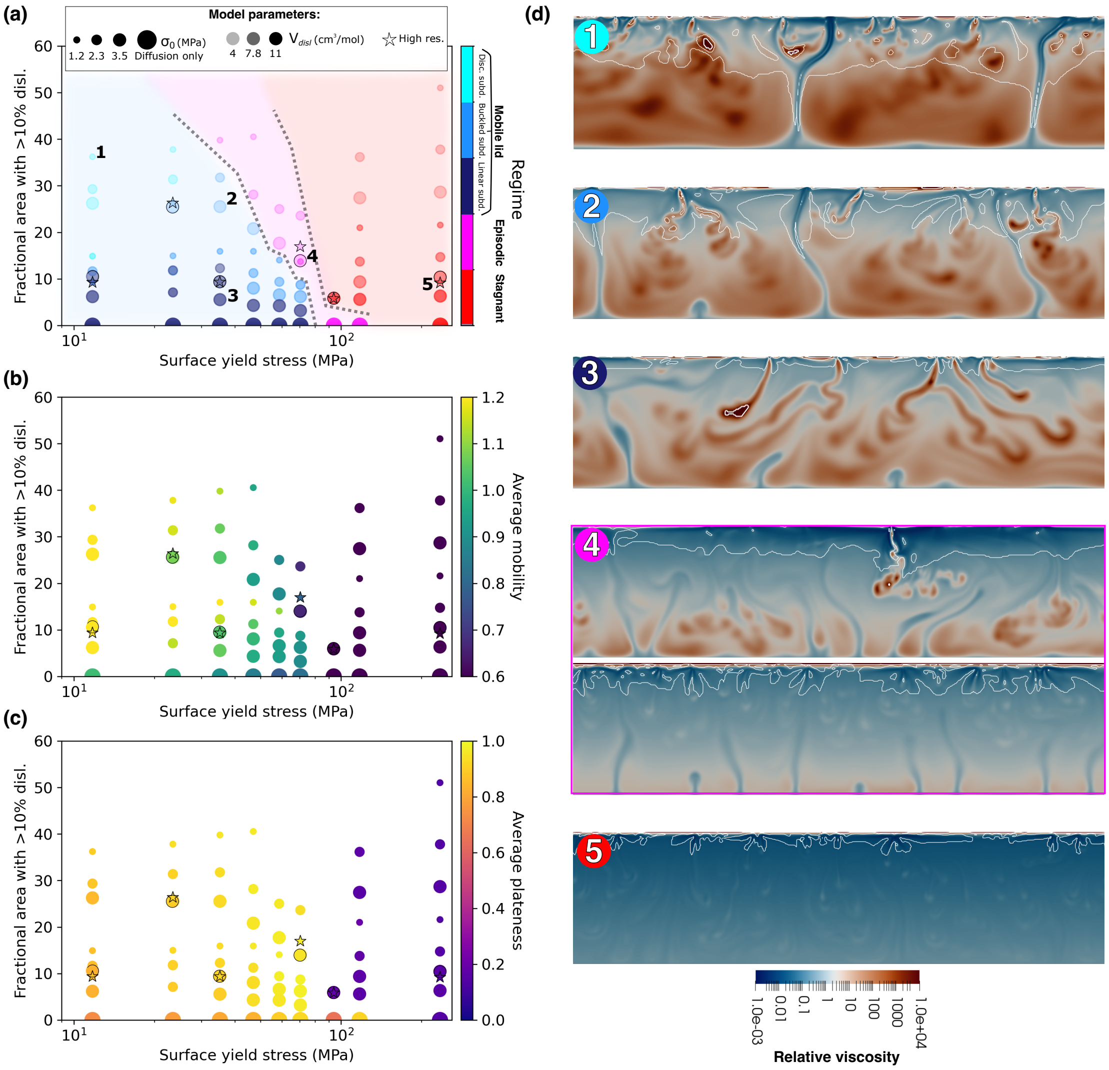

Figure 4. (a) Regime diagram of all models. Mobile-lid models have discontinuous and short-lived subductions (cyan), buckled slabs (blue), or mostly linear slabs (deep-blue). Episodic models (magenta) have intermediate plateness and mobility. Stagnant-lid models (red) have low plateness and mobility. Qualitative boundaries are drawn between each regime. (b-c) Similar to (a) but with colours representing time-averaged surface mobility and plateness, respectively. (d) Snapshots of viscosity of selected models referred as numbers in (a). White lines contour low-viscosity regions with >10% dislocation creep.

pling contributes to the observed increase in mobility. Since dislocation creep also favors lithosphere thinning, the plastic strength at lithospheric base is reduced compared to models in pure diffusion creep. Therefore, an increasing amount of dislocation creep enhances thin slab break-offs. Accounting for composite rheology in models with a low lithospheric strength thus enhances mobile-lid convection.

3.2.2 Models with a strong lithosphere (>35 MPa)

Models in pure diffusion creep with surface yield stresses comprised between ∼35 MPa and ∼120 MPa are also still in the mobile-lid regime. Including composite rheology with decreasing values of V_{disl} and/or σ_0 results in up to 40 % of the mantle being affected by dislocation creep (Fig. 3b and 4a-c).

For small amounts of dislocation creep in the mantle (<20%), both plateness and surface mobility tend to increase by a factor of up to 1.4 and the number of slabs remains stable (Fig. 3b). In these models, thin low-viscosity asthenospheric areas tend to lubricate the base of the lithosphere, enhancing plate mobility and plateness (e.g. Tackley, 2000b).

When the proportion of dislocation creep exceeds 20%, the number of active subductions, plateness, and surface mobility decrease (Fig. 3b, 4a-c, and S5b). Lithosphere-asthenosphere decoupling promotes episodic and stagnant-lid convection (Fig. 4). This strengthening phenomenon due to large viscosity contrasts between the convecting mantle and the lithosphere has long been demonstrated using Newtonian rheology (e.g. Moresi & Solomatov, 1995; Solomatov, 1995; Höink et al., 2012, although the latter study invoked a flow channelization effect as being responsible for stagnant-lid convection) and non-Newtonian rheology in the asthenosphere (Semple & Lenardic, 2020, although they did not employ temperature- and depth-dependent viscosity, in contrast to the present study).

We further tested higher surface yield stresses (>120 MPa), which led to continuous stagnant-lid behavior irrespective of our choice of activation parameters. Like in models with a lower yield stress, decreasing V_{disl} and/or σ_0 produces a thickening of the layer containing dislocation creep. Although the convective regime remains unchanged in these models, changing the amount of dislocation creep can strongly decrease the viscosity in the asthenosphere and decrease lithospheric thickness by up to 60%. These effects could have a large impact on the distribution of partial melting and the rates of magmatism on stagnant-lid planets (e.g. Schulz et al., 2020; Tosi & Padovan, 2021). However, these models also suggest that once a stagnant-lid is established with a pure diffusion creep rheology, adding composite rheology in the upper-mantle does not promote the generation of more plate-like behavior.

4 Discussion and conclusion

4.1 Model assumptions

Model setup simplifications potentially alter mantle flow and therefore the spatio-temporal diffusion/dislocation creep partitioning. Our models are limited to 2D-cartesian, have a reference Rayleigh number ∼10 times lower than Earth's, lower lithospheric strengths than inferred from laboratory experiments (e.g. Brace & Kohlstedt, 1980), and lower activation parameters for olivine than those predicted by rock experiments (e.g. Hirth & Kohlstedt, 2003). We do not consider multiple mantle and lithosphere compositions and phases (e.g. King, 2016). We also only tested one initial thermal state for our models with composite rheology although different initial conditions could lead to distinct regime boundaries for diffusion-creep-only and composite rheology, as shown in e.g. Semple and Lenardic (2021); Weller and Lenardic (2018).

However, our mobile-lid models still produce mantle velocities of the order of the cm/yr (Fig. 2a), oceanic lithosphere thickness of 100-200 km, and successfully generate dislocation creep where it is expected to occur from rock-deformation experiments (Fig. 1). We also note no significant difference when increasing the resolution (Fig. 4a-c, star symbols). Therefore, we anticipate that the general convective and tectonic trends (Fig. 4) and physical mechanisms described in this study still apply using more Earth-like setups. In particular, we obtain a self-generated and self-evolving low-viscosity asthenosphere without invoking water and/or partial melting (King, 2016; Semple & Lenardic, 2020), the latter being often called on to justify the use of weakening laws to improve plateness in whole-mantle Newtonian models (e.g. Tackley, 2000a; Bello et al., 2015).

Importantly, we assumed a uniform static grain-size, although rock-deformation experiments indicate that diffusion creep should strongly depend on grain-size evolution (Eq. 1). In some stagnant-lid models, we increased the static grain size, which produced an increase in mantle average viscosity, stress, and proportion of dislocation creep in the uppermost mantle (Fig. S6), associated with lithospheric thickening, as already described in Schulz et al. (2020). This test, applied to models without dynamic grain-growth and reduction, reveals the competing effects of large grain size (which tends to increase mantle viscosity) and large amounts of dislocation creep (which tend to decrease it) on lithosphere thickness, at least up to a doubling of static grain-size with our setup (Fig. S6). Further exploring the role of grain-size evolution in mobile-lid scenarios is therefore needed to further understand the role of composite rheology on mantle and lithosphere dynamics.

4.2 Earth's observations and composite rheology in the uppermost mantle

On Earth, seismic anisotropy, through the generation of dislocation creep-induced LPO (e.g. Nicolas & Christensen, 1987), can provide complementary insight on the lateral variations of mantle rheological properties (e.g. Becker et al., 2008). Although 3D modeling is required to quantitatively compare the diffusion/dislocation creep partitioning in our models with observed seismic anisotropy, our results already potentially explain its observed orientation and strength variations (e.g. Debayle et al., 2005), as well as high strength around slabs (e.g. Jadamec & Billen, 2012) and in the thermal trail of plumes (e.g. Barruol et al., 2019). The correlation between strong anisotropy and fast plate velocities described in Debayle and Ricard (2013) could also partly result from the fact that these plates are attached to fast sinking slabs, thus favoring more dislocation creep due to lithosphere basal shear. One future direction would therefore be to estimate seismic anisotropy in more Earth-like models with composite rheology and compare it to Earth's observations (e.g. Kendall et al., 2022). Together with the consideration that some rheological parameters are inter-dependent (e.g. Jain et al., 2019), this should provide complementary constraints on the range of rheological parameters applicable to Earth. Finally, another independent constraint could come from the study of how composite rheology affects the spatio-temporal distribution of surface dynamic topography, both on the long-term (e.g. Bodur & Rey, 2019) and on shorter glacial-isostatic-adjustment timescales (Kang et al., 2022).

In this study, we show that our choice of composite rheological parameters impacts uppermost mantle spatio-temporal viscosity variations and dynamics, therefore affecting convection and surface tectonics in a non-linear way: at low lithospheric strength, increasing the proportion of mantle deforming through dislocation creep promotes plate mobility as well as numerous, weaker and short-lived slabs. In contrast, increasing the proportion of mantle containing dislocation creep in models with large lithospheric strength, results in episodic to stagnant-lid convection. This shows the potential geodynamical influence of experimental uncertainties of the rheological parameters and calls for both further experimental refinement of mantle rheological parameters such as V_{disl}, and further exploration of the effects of composite rheology on mantle convective planform and surface tectonics in more sophisticated planetary-scale models.

Open Research

The convection code StagYY (Tackley, 2008) is property of ETH Zurich and Paul J. Tackley. Data files used in this study can be downloaded from Arnould (2022).

Acknowledgments

This research benefited from Norwegian Research Council funding to the Centre for Earth Evolution and Dynamics (223272) and to TR (PLATONICS, 276032). MA benefited from INSU-PNP and UCBL-BQR fundings. Computations were performed on Stallo and Saga Uninett Sigma2 facilities (nn9010k, ns9010k). Crameri et al. (2020) authored Fig.4d colormap.

References

Alisic, L., Gurnis, M., Stadler, G., Burstedde, C., & Ghattas, O. (2012). Multi-scale dynamics and rheology of mantle flow with plates. *Journal of Geophysical Research: Solid Earth*, *117*(B10), 148–227. doi: https://doi.org/10.1029/2012JB009234

Allmann, B. P., & Shearer, P. M. (2009). Global variations of stress drop for moderate to large earthquakes. *Journal of Geophysical Research: Solid Earth*, *114*(B1).

Arnould, M. (2022, Apr). *Effects of composite rheology on plate-like behaviour in global-scale mantle convection [dataset].* OSF. Retrieved from `osf.io/p3mvn`

Arnould, M., Coltice, N., Flament, N., Seigneur, V., & Muller, R. D. (2018). On the scales of dynamic topography in whole-mantle convection models. *Geochemistry, Geophysics, Geosystems*, *19*(9), 3140-3163.

Asaadi, N., Ribe, N. M., & Sobouti, F. (2011). Inferring nonlinear mantle rheology from the shape of the hawaiian swell. *Nature*, *473*(7348), 501–504.

Barruol, G., Sigloch, K., Scholz, J.-R., Mazzullo, A., Stutzmann, E., Montagner, J.-P., ... others (2019). Large-scale flow of indian ocean asthenosphere driven by réunion plume. *Nature Geoscience*, *12*(12), 1043–1049.

Becker, T. W., Chevrot, S., Schulte-Pelkum, V., & Blackman, D. K. (2006). Statistical properties of seismic anisotropy predicted by upper mantle geodynamic models. *Journal of Geophysical Research: Solid Earth*, *111*(B8).

Becker, T. W., Kustowski, B., & Ekström, G. (2008). Radial seismic anisotropy as a constraint for upper mantle rheology. *Earth and Planetary Science Letters*, *267*(1-2), 213–227.

Beghein, C., Yuan, K., Schmerr, N., & Xing, Z. (2014). Changes in seismic anisotropy shed light on the nature of the gutenberg discontinuity. *Science*, *343*(6176), 1237–1240.

Bello, L., Coltice, N., Tackley, P. J., Müller, R. D., & Cannon, J. (2015). Assessing the role of slab rheology in coupled plate-mantle convection models. *Earth and Planetary Science Letters*, *430*, 191–201.

Billen, M. I., & Hirth, G. (2005). Newtonian versus non-newtonian upper mantle viscosity: Implications for subduction initiation. *Geophysical Research Letters*, *32*(19). doi: https://doi.org/10.1029/2005GL023457

Billen, M. I., & Hirth, G. (2007). Rheologic controls on slab dynamics. *Geochemistry, Geophysics, Geosystems*, *8*(8). doi: https://doi.org/10.1029/2007GC001597

Bodur, Ö. F., & Rey, P. F. (2019). The impact of rheological uncertainty on dynamic topography predictions. *Solid Earth*, *10*(6), 2167–2167.

Brace, W. F., & Kohlstedt, D. L. (1980). Limits on lithospheric stress imposed by laboratory experiments. *Journal of Geophysical Research: Solid Earth*, *85*(B11), 6248-6252. Retrieved from `https://agupubs.onlinelibrary.wiley.com/doi/abs/10.1029/JB085iB11p06248` doi: https://doi.org/10.1029/JB085iB11p06248

Christensen, U. (1983). Convection in a variable-viscosity fluid: Newtonian versus power-law rheology. *Earth and Planetary Science Letters*, *64*(1), 153–162.

Christensen, U. (1984). Convection with pressure-and temperature-dependent non-newtonian rheology. *Geophysical Journal International*, *77*(2), 343–384.

Coltice, N., Gérault, M., & Ulvrová, M. (2017). A mantle convection perspective on global tectonics. *Earth-science reviews*, *165*, 120–150.

Crameri, F., Shephard, G. E., & Heron, P. J. (2020). The misuse of colour in science communication. *Nature communications*, *11*(1), 1–10.

Dannberg, J., Eilon, Z., Faul, U., Gassmöller, R., Moulik, P., & Myhill, R. (2017). The importance of grain size to mantle dynamics and seismological observations. *Geochemistry, Geophysics, Geosystems*, *18*(8), 3034–3061.

Debayle, E., Kennett, B., & Priestley, K. (2005). Global azimuthal seismic anisotropy and the unique plate-motion deformation of australia. *Nature*, *433*(7025), 509–512.

Debayle, E., & Ricard, Y. (2013). Seismic observations of large-scale deformation at the bottom of fast-moving plates. *Earth and Planetary Science Letters*, *376*, 165–177.

Garel, F., Thoraval, C., Tommasi, A., Demouchy, S., & Davies, D. R. (2020). Using thermo-mechanical models of subduction to constrain effective mantle viscosity. *Earth and Planetary Science Letters*, *539*, 116243. doi: https://doi.org/10.1016/j.epsl.2020.116243

Hall, C. E., & Parmentier, E. (2003). Influence of grain size evolution on convective instability. *Geochemistry, Geophysics, Geosystems*, *4*(3). doi: https://doi.org/10.1029/2002GC000308

Hedjazian, N., Garel, F., Davies, D. R., & Kaminski, E. (2017). Age-independent seismic anisotropy under oceanic plates explained by strain history in the asthenosphere. *Earth and Planetary Science Letters*, *460*, 135–142.

Hirth, G., & Kohlstedt, D. (2003). Rheology of the upper mantle and the mantle wedge: A view from the experimentalists. *Geophysical Monograph-American Geophysical Union*, *138*, 83–106.

Höink, T., Lenardic, A., & Richards, M. (2012). Depth-dependent viscosity and mantle stress amplification: implications for the role of the asthenosphere in maintaining plate tectonics. *Geophysical Journal International*, *191*(1), 30–41.

Holt, A. F., & Becker, T. W. (2016). The effect of a power-law mantle viscosity on trench retreat rate. *Geophysical Journal International*, 491–507.

Jadamec, M., & Billen, M. (2010). Reconciling surface plate motions with rapid three-dimensional mantle flow around a slab edge. *Nature*, *465*(7296), 338–341.

Jadamec, M., & Billen, M. I. (2012). The role of rheology and slab shape on rapid mantle flow: Three-dimensional numerical models of the alaska slab edge. *Journal of Geophysical Research: Solid Earth*, *117*(B2). doi: https://doi.org/10.1029/2011JB008563

Jain, C., Korenaga, J., & Karato, S.-i. (2018). On the grain size sensitivity of olivine rheology. *Journal of Geophysical Research: Solid Earth*, *123*(1), 674–688.

Jain, C., Korenaga, J., & Karato, S.-i. (2019). Global analysis of experimental data on the rheology of olivine aggregates. *Journal of Geophysical Research: Solid Earth*, *124*(1), 310–334.

Kang, K., Zhong, S., Geruo, A., & Mao, W. (2022). The effects of non-newtonian rheology in the upper mantle on relative sea level change and geodetic observables induced by glacial isostatic adjustment process. *Geophysical Journal International*, *228*(3), 1887–1906.

Karato, S.-i., & Wu, P. (1993). Rheology of the upper mantle: A synthesis. *Science*, *260*(5109), 771–778.

Kendall, E., Faccenda, M., Ferreira, A., & Chang, S.-J. (2022). On the relationship between oceanic plate speed, tectonic stress, and seismic anisotropy. *Geophysical Research Letters*, *49*(15), e2022GL097795.

King, S. D. (2016). An evolving view of transition zone and midmantle viscosity. *Geochemistry, Geophysics, Geosystems*, *17*(3), 1234–1237.

Korenaga, J., & Karato, S.-I. (2008). A new analysis of experimental data on olivine rheology. *Journal of Geophysical Research: Solid Earth*, *113*(B2).

Li, M., & Zhong, S. (2019). Lateral motion of mantle plumes in 3-d geodynamic models. *Geophysical Research Letters*, *46*(9), 4685–4693.

Moresi, L.-N., & Solomatov, V. (1995). Numerical investigation of 2d convection with extremely large viscosity variations. *Physics of Fluids*, *7*(9), 2154–2162.

Neuharth, D., & Mittelstaedt, E. (2023). Temporal variations in plume flux: characterizing pulsations from tilted plume conduits in a rheologically complex mantle. *Geophysical Journal International*, *233*(1), 338–358.

Nicolas, A., & Christensen, N. I. (1987). Formation of anisotropy in upper mantle peridotites-a review. *Composition, structure and dynamics of the lithosphere-asthenosphere system*, *16*, 111–123.

Phipps Morgan, J., Morgan, W. J., Zhang, Y.-S., & Smith, W. H. (1995). Observational hints for a plume-fed, suboceanic asthenosphere and its role in mantle convection. *Journal of Geophysical Research: Solid Earth*, *100*(B7), 12753–12767.

Ranalli, G. (2001). Mantle rheology: radial and lateral viscosity variations inferred from microphysical creep laws. *Journal of Geodynamics*, *32*(4-5), 425–444.

Rolf, T., Capitanio, F. A., & Tackley, P. J. (2018). Constraints on mantle viscosity structure from continental drift histories in spherical mantle convection models. *Tectonophysics*, *746*, 339–351.

Rozel, A. (2012). Impact of grain size on the convection of terrestrial planets. *Geochemistry, Geophysics, Geosystems*, *13*(10). doi: https://doi.org/10.1029/2012GC004282

Schulz, F., Tosi, N., Plesa, A.-C., & Breuer, D. (2020). Stagnant-lid convection with diffusion and dislocation creep rheology: Influence of a non-evolving grain size. *Geophysical Journal International*, *220*(1), 18–36.

Semple, A., & Lenardic, A. (2020). The robustness of pressure-driven asthenospheric flow in mantle convection models with plate-like behavior. *Geophysical Research Letters*, *47*(17), e2020GL089556.

Semple, A., & Lenardic, A. (2021). Feedbacks between a non-newtonian upper mantle, mantle viscosity structure and mantle dynamics. *Geophysical Journal International*, *224*(2), 961–972.

Solomatov, V. (1995). Scaling of temperature-and stress-dependent viscosity convection. *Physics of Fluids*, *7*(2), 266–274.

Stein, C., Schmalzl, J., & Hansen, U. (2004). The effect of rheological parameters on plate behaviour in a self-consistent model of mantle convection. *Physics of the Earth and Planetary Interiors*, *142*(3-4), 225–255.

Tackley, P. J. (2000a). Self-consistent generation of tectonic plates in time-dependent, three-dimensional mantle convection simulations. *Geochemistry, Geophysics, Geosystems*, *1*(8). doi: https://doi.org/10.1029/2000GC000036

Tackley, P. J. (2000b). Self-consistent generation of tectonic plates in time-dependent, three-dimensional mantle convection simulations 2. strain weakening and asthenosphere. *Geochemistry, Geophysics, Geosystems*, *1*(8). doi: https://doi.org/10.1029/2000GC000043

Tackley, P. J. (2008). Modelling compressible mantle convection with large viscosity contrasts in a three-dimensional spherical shell using the yin-yang grid. *Physics* *of the Earth and Planetary Interiors*, *171*(1-4), 7–18. doi: https://doi.org/10.1016/j.pepi.2008.08.005

Tosi, N., & Padovan, S. (2021). Mercury, moon, mars. In *Mantle convection and surface expressions* (p. 455-489). American Geophysical Union (AGU). Retrieved from https://agupubs.onlinelibrary.wiley.com/doi/abs/10.1002/9781119528609.ch17 doi: https://doi.org/10.1002/9781119528609.ch17

Trompert, R., & Hansen, U. (1998). Mantle convection simulations with rheologies that generate plate-like behaviour. *Nature*, *395*(6703), 686–689.

Weller, M. B., & Lenardic, A. (2018). On the evolution of terrestrial planets: Bi-stability, stochastic effects, and the non-uniqueness of tectonic states. *Geoscience Frontiers*, *9*(1), 91–102.

Supporting Information for "Effects of mantle composite rheology on plate-like behavior in global-scale mantle convection"

M. Arnould[1,2], T. Rolf[2,3]and A. Manjón Cabeza-Córdoba [2,4,5]

[1]UCBL, ENSL, UJM, CNRS 5276, Laboratoire de Géologie de Lyon - Terre, Planètes, Environnement, Lyon, France

[2]Centre for Earth Evolution and Dynamics, Department of Geosciences, University of Oslo, Blindern, Oslo, Norway

[3]Institute of Geophysics, University of Münster, Germany

[4]Andalusian Earth Sciences Institute, University of Grenada, Spain

[5]Department of Earth Sciences, University College London, UK

Contents of this file

1. Table S1

2. Figures S1 to S6

Additional Supporting Information (Files uploaded separately)

1. Supplementary Movie 1: Spatio-temporal distribution of dislocation creep and mantle velocity field (arrows scaled and colored by magnitude) in a model of mantle convection with composite rheology (same model as Fig. 2c). Blue lines show slabs (isotherm 1375 K) and magenta lines contour plumes (isotherm 2000 K).

Table S1. Non-dimensional and dimensional model parameters

Parameter	Non-dim. value	Dim. value	Scaling[a]
Mantle thickness (D)	1	2890 km	
Reference gravitational acceleration (g_0)	1	9.81 m s^{-2}	
Reference thermal expansivity (α_0)	1	5×10^{-5} K^{-1}	
Reference density (ρ_0)	1	3300 kg m^{-3}	
Reference diffusivity (κ_0)	1	1×10^{-6} m^2 s^{-1}	
Temperature gradient (ΔT)	1	2500 K	
Surface temperature (T$_{top}$)	0.12	300 K	ΔT
Basal temperature (T$_{bot}$)	1.12	2800 K	ΔT
Reference viscosity (η_0)	1	9.8×10^{21} Pa s	$\frac{\alpha_0 g_0 \rho_0 \Delta T D^3}{\kappa \mathrm{Ra}_0}$
Internal heating rate (H)	30	8.6×10^{-12} W kg^{-1}	$\frac{k_0 \Delta T}{\rho_0 D^2}$
Diffusion creep activation energy (E_{diff})	6	125 kJ mol^{-1}	$R\Delta T$
Diffusion creep activation volume (V_{diff})	3	0.7 cm^3 mol^{-1}	$\frac{R\Delta T}{\rho_0 g_0 D}$
Stress exponent for diffusion creep (n)	0		
Grain-size exponent for diffusion creep (m)	2		
Dislocation creep activation energy (E_{disl})	11	230 kJ mol^{-1}	$R\Delta T$
Dislocation creep activation volume (V_{disl})	18 – 50	4 – 11 cm^3 mol^{-1}	$\frac{R\Delta T}{\rho_0 g_0 D}$
Stress exponent for dislocation creep (n)	3.5		
Grain-size exponent for dislocation creep (m)	1		
Reference transition stress (σ_0)	$1 - 3 \times 10^3$	1.2 – 3.5 MPa	$\frac{\kappa_0 \eta_0}{D^2}$
Maximum viscosity cut-off	10^4	9.8×10^{25} Pa s	
Surface yield stress (σ_{Y_0})	$1 - 20 \times 10^4$	12 – 234 MPa	$\frac{\kappa_0 \eta_0}{D^2}$
Yield stress gradient (dσ_Y)	0.01	0.325 MPa km^{-1}	$\frac{Ra_0}{\alpha_0 \Delta T} \frac{\kappa_0 \eta_0}{D^3}$

[a] The scaling factors listed in this column need to be multiplied by the non-dimensional values to get the dimensional parameters. $\mathrm{Ra}_0 = 10^7$ is the reference Rayleigh number, $R = 8.314$ kJ mol^{-1} is the gas constant and $k_0 = 3.15$ W m^{-1} K^{-1} is the reference thermal conductivity. Velocities are dimensionalized using D and the thermal diffusion time ($\tau = \frac{D^2}{\kappa}$).

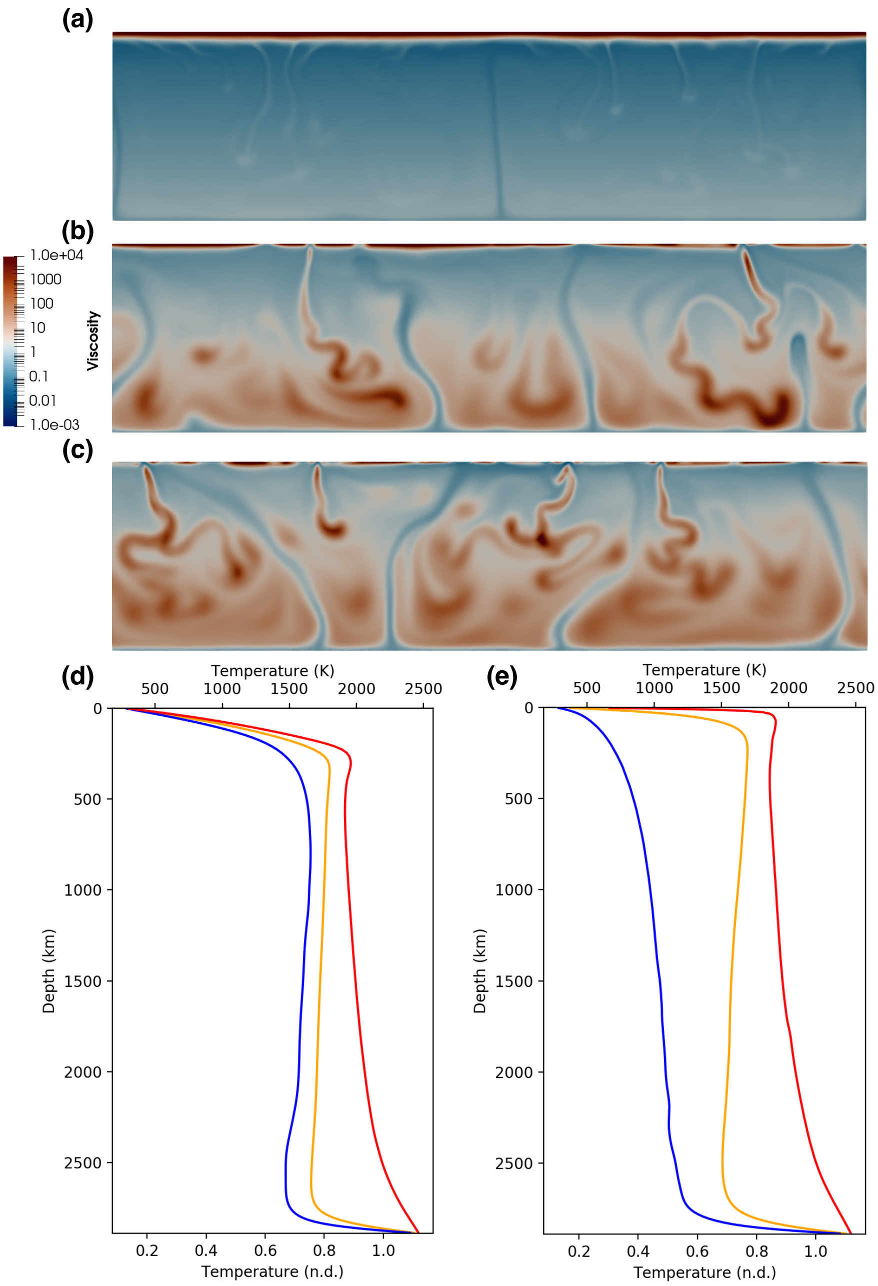

Figure S1. Snapshots (a-b-c) of the viscosity fields of three 2D-cartesian models with different yield stresses (σ_{Y_0} equal to 234 MPa, 47 MPa and 12 MPa respectively), deforming in diffusion creep only. (d) and (e) show the time-averaged temperature profiles of (a) and (b) respectively. The blue, yellow and red curves correspond to the time-averaged minimum, mean and maximum temperature profiles. (a) and (d) correspond to a stagnant-lid model while (b), (c) and (e) correspond to mobile-lid models with plate-like behavior.

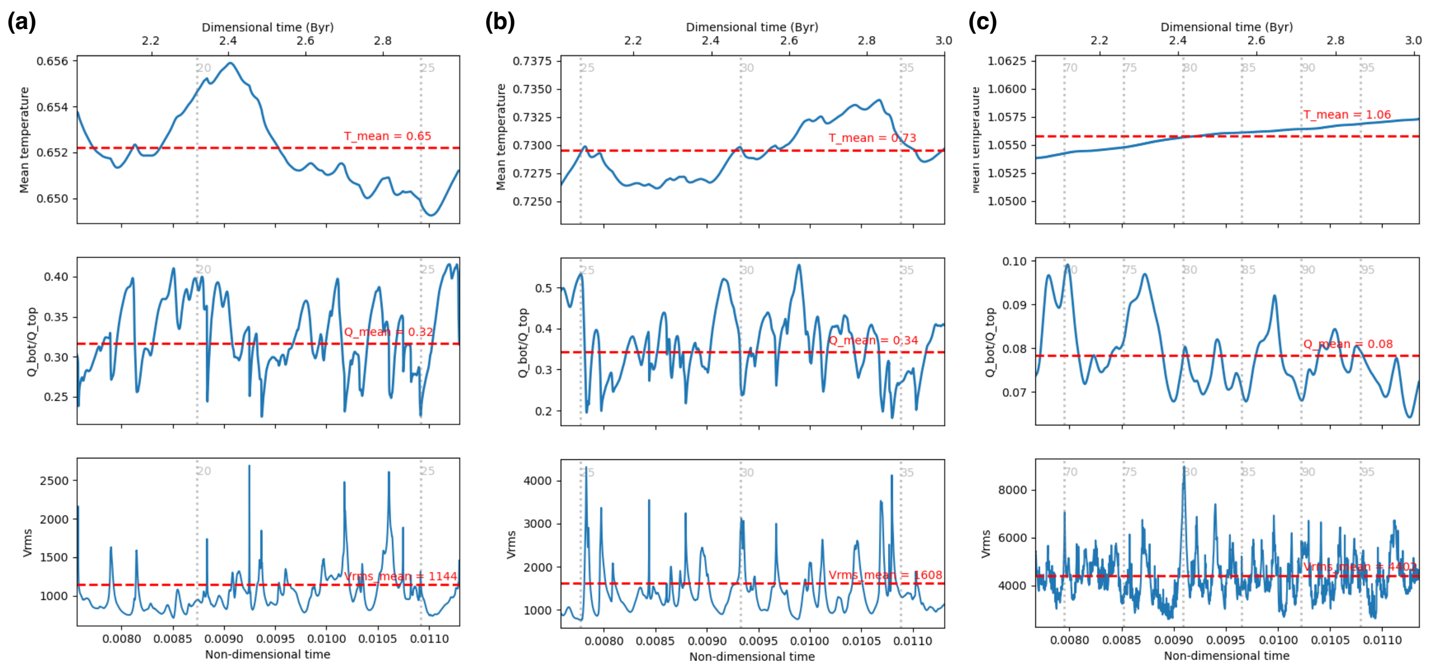

Figure S2. Time series of non-dimensional temperature, bottom/surface heat flow ratio and rms velocities for models (a) with $\sigma_{Y_0} = 12$ MPa, $V_{disl} = 11$ cm^3/mol and $\sigma_0 = 3.5$ MPa, (b) $\sigma_{Y_0} = 35$ MPa, $V_{disl} = 11$ cm^3/mol and $\sigma_0 = 3.5$ MPa, and (c) $\sigma_{Y_0} = 234$ MPa, $V_{disl} = 4$ cm^3/mol and $\sigma_0 = 3.5$ MPa. The red line corresponds to the average of each time series. The dotted grey lines represent specific overturns and correspond to the amount of time necessary for a particle to sink from the surface to the base of the mantle and then back to the surface at the average rms velocity of the corresponding model. Non-dimensional time is dimensionalized using diffusivity: $t_{dim} = t * \times \frac{D^2}{\kappa_0}$.

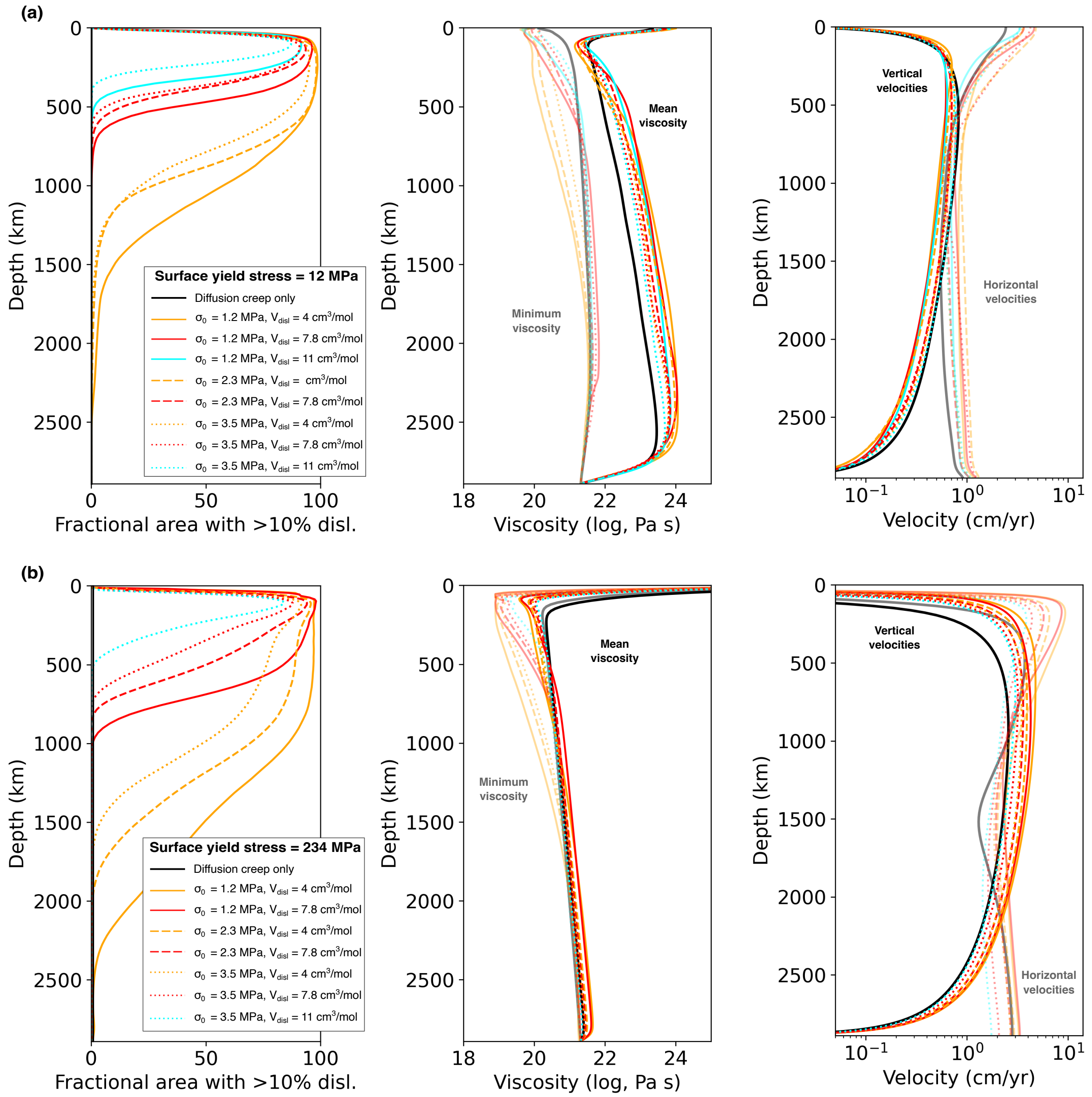

Figure S3. Same depth-profiles as Fig. 2a, but (a) for a low surface yield stress), and (b) for a high surface yield stress. Although the absolute values of viscosity change with the surface yield stress for model in pure diffusion creep due to regime transition from mobile lid (cool and viscous) at 12 MPa to stagnant lid (hot) at 234 MPa, accounting for different amounts of dislocation creep generally has a lowering effect on mantle viscosity.

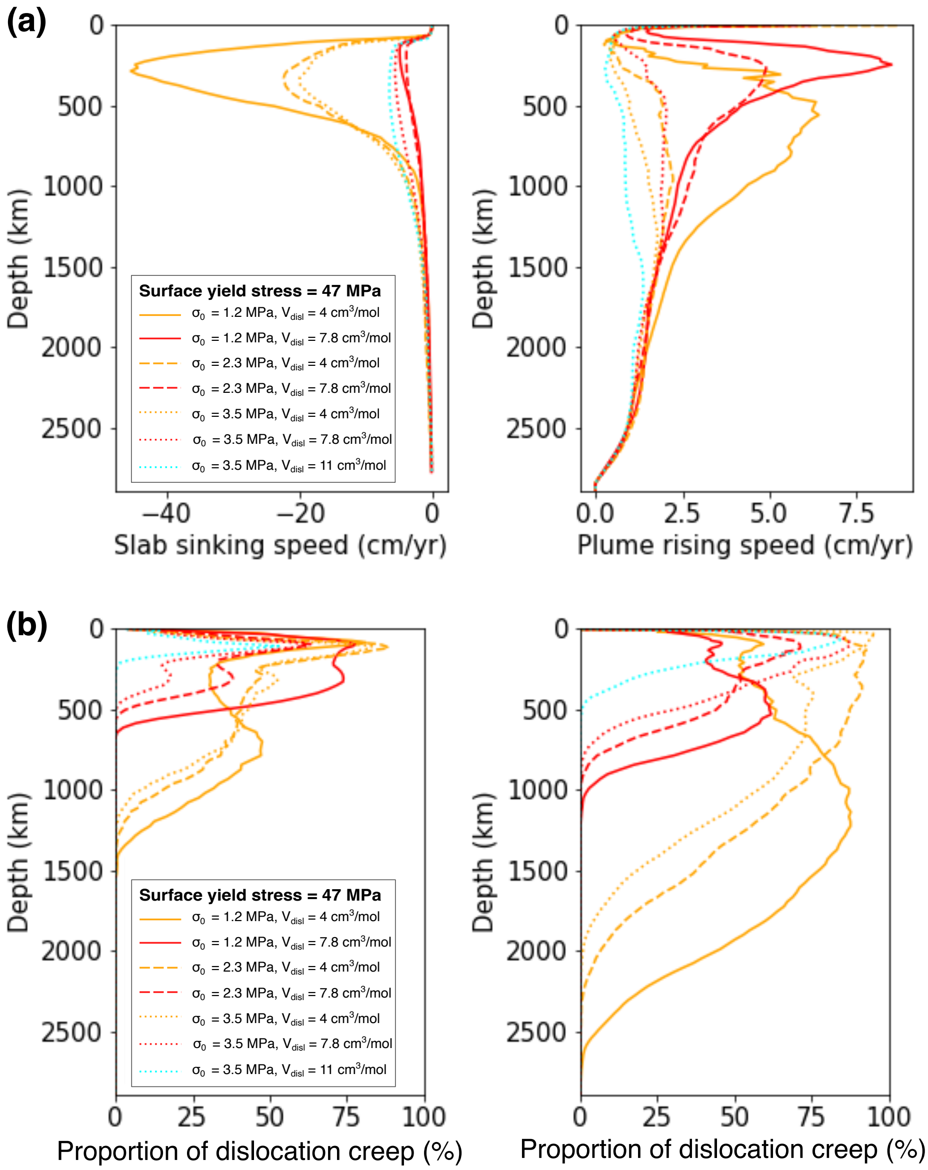

Figure S4. Rheological properties and behavior inside slabs (left panels) and plumes (right panel) in composite rheology models with a surface yield stress of 47 MPa. Time-averaged depth profiles of (a) sinking/rising speed and (b) proportion of slab/plume material deforming through dislocation creep. Note the increasing vertical velocity with increasing proportion of dislocation creep.

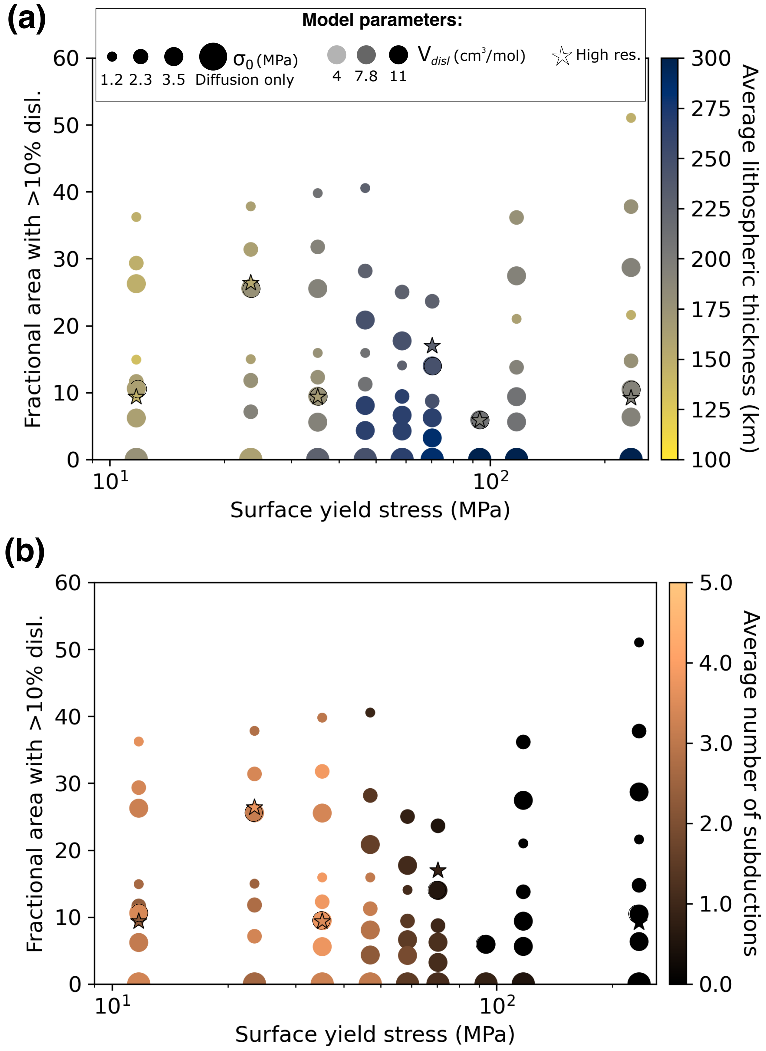

Figure S5. Regime diagram as shown on Figure 4 of the main manuscript, but with colours referring to (a) time-averaged lithosphere thickness and (b) to the average number of subductions. Note the progressive increase of lithospheric thickness in models in pure diffusion creep as the surface yield stress increases. Also note that for a given surface yield stress, the increase in the mantle fractional area containing more than 10 % dislocation creep leads to progressive lithosphere thinning. Models with a surface yield stress lower than 50 MPa tend to exhibit more subductions when increasing the amount of mantle deforming through dislocation creep compared to models with diffusion creep only.

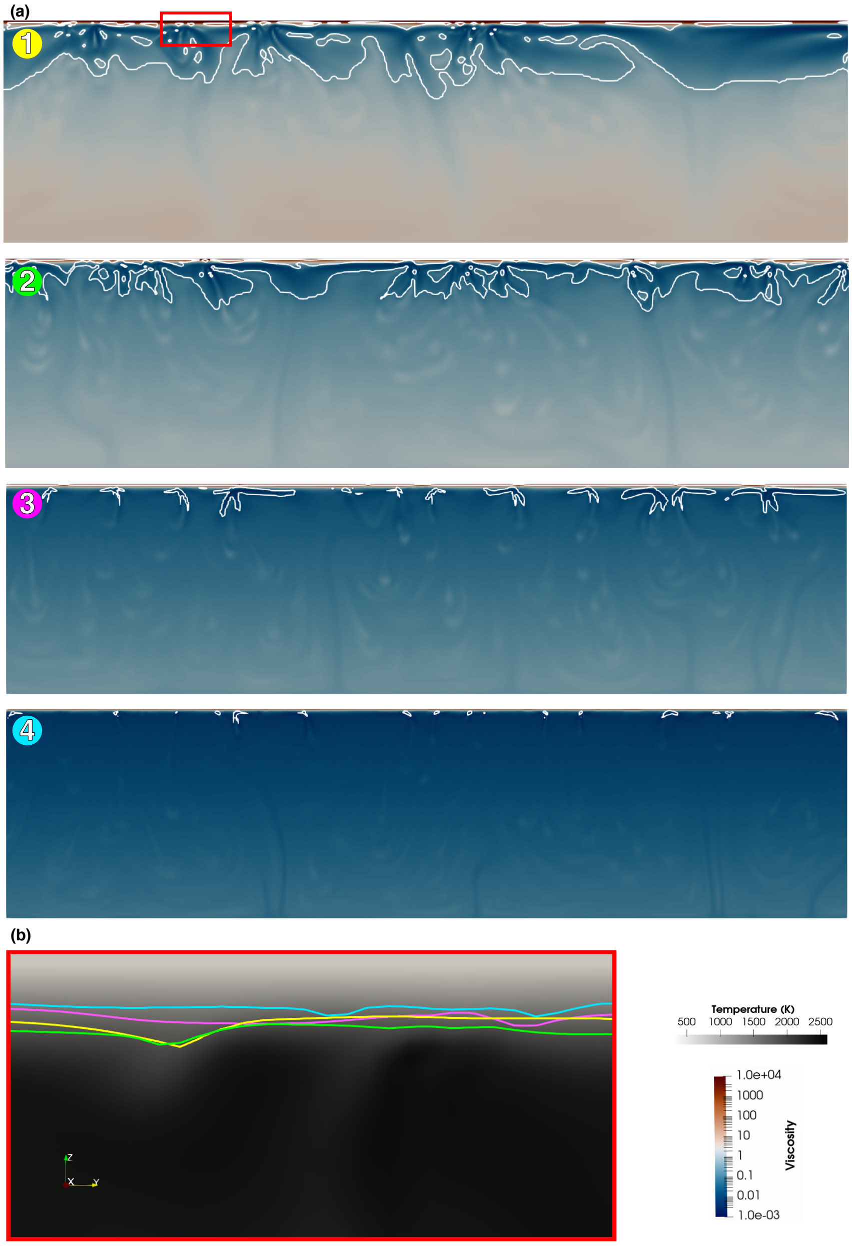

Figure S6. Effect of static grainsize on the planform of convection, on the proportion of dislocation creep and on the lithospheric thickness in stagnant-lid models. (a) Snapshots of the viscosity field for 4 models with composite rheology (V_{disl} = 7.8 cm^3 mol^{-1} and σ_0 = 3.5 MPa). In models 1, 2, and 4 the grain size is 4x, 2x, and 0.5x the grain size in model 3, respectively. White lines contour low-viscosity areas deforming 100% in dislocation creep. (b) Zoom in on the temperature field of Model 1 (red square on (a.1)) showing the location of the isotherm 1700 K for all models at the end of the simulations.